6888

NACA TN 2502

TECH LIBRARY KAFB, NM
0065504

NATIONAL ADVISORY COMMITTEE FOR AERONAUTICS

TECHNICAL NOTE 2502

EXAMPLES OF THREE REPRESENTATIVE TYPES OF AIRFOIL-SECTION STALL AT LOW SPEED

By George B. McCullough and Donald E. Gault

Ames Aeronautical Laboratory
Moffett Field, Calif.

Washington

September 1951

AFMDC
TECHNICAL LIBRARY
AFL 2811

TECH LIBRARY KAFB, NM
0065504

NATIONAL ADVISORY COMMITTEE FOR AERONAUTICS

TECHNICAL NOTE 2502

EXAMPLES OF THREE REPRESENTATIVE TYPES OF AIRFOIL-SECTION STALL AT LOW SPEED

By George B. McCullough and Donald E. Gault

SUMMARY

Force, moment, pressure-distribution, and boundary-layer measurements are presented for a series of five airfoil sections. The stalling characteristics of these airfoil sections at low speeds are of three types:

1. Trailing-edge stall (preceded by movement of the turbulent separation point forward from the trailing edge with increasing angle of attack)

2. Leading-edge stall (abrupt flow separation near the leading edge generally without subsequent reattachment)

3. Thin-airfoil stall (preceded by flow separation at the leading edge with reattachment at a point which moves progressively rearward with increasing angle of attack)

The role of the boundary-layer flow and separation processes in relation to stalling as well as the sensitivity of the stall to factors which influence boundary-layer growth, such as Reynolds number, is discussed.

INTRODUCTION

The variables involved in the stall[1] of a complete wing are many, and include the factors of airfoil shape, wing plan form, wing twist, fuselage and nacelle interference, surface roughness, stream turbulence, and Reynolds number. A direct attack on the problem of wing stall is, therefore, a formidable undertaking. Since the stall results from boundary-layer separation, a complete understanding of the stall depends on an

[1]For the purposes of this report the stall is defined as the flow condition which follows the first lift-curve peak.

understanding of the mechanics of boundary-layer separation, a phenomenon which has not been fully explained to date, and which is beyond the scope of the present report. Considerable insight into the problem of wing stalling may be gained, however, by observing the processes of boundary-layer separation in two-dimensional flow fields. A study of the stalling characteristics of airfoil sections is, therefore, an important phase of the over-all problem of wing stalling and can greatly assist the airplane designer in the selection of airfoil sections for specific applications.

It is the purpose of the present report to summarize the stalling characteristics of a series of five symmetrical airfoil sections based on investigations conducted in the Ames 7- by 10-foot wind tunnels. The stalling of these airfoils is classified into three general types, and illustrative examples of the force, moment, pressure-distribution, and boundary-layer characteristics of each type are discussed in detail. The data are directly comparable with one another because similar testing techniques and models were employed in all investigations. Most of the ideas contained herein are now new, but the presentation furnishes a compilation of some of the more significant knowledge on the subject of airfoil-section stalling and associated two-dimensional flow phenomena.

HISTORICAL BACKGROUND

Beginning about 1930, as a result of intensive wind-tunnel investigations of the effects of Reynolds number and stream turbulence, the role of the boundary layer in stalling became of interest and was subjected to direct observations. This work is typified by references 1 and 2. In 1931, Jacobs speculated that the shape of the lift-curve peak was controlled by the position and movement of the point of separation of turbulent flow on the airfoil surface. Shortly thereafter one of the earliest efforts to correlate the type of boundary-layer flow and separation with stalling was reported by Millikan and Klein. They suggested, after investigating the effect of turbulence on maximum lift, that the point of transition from laminar to turbulent flow relative to the point of laminar separation was critical in determining maximum lift. They pointed out that if transition moves ahead of the theoretical point of laminar separation, then the laminar stall cannot occur, and increased values of maximum lift might be realized because the turbulent boundary layer resists separation to a much greater extent than does the laminar boundary layer.

Contemporaneously with the work reported in references 1 and 2, B. Melvill Jones investigated the stalling characteristics of several different airfoil sections experimentally and made what is apparently the first generalization of stalling characteristics (references 3 and 4). He classified stalling into three types: a trailing-edge stall, and two types of leading-edge stall. Jones' significant conclusion was that

stalling could result from flow separation at the leading edge as well as from the trailing edge of an airfoil. Perhaps equally important, although seemingly overlooked at the time, was his observation of the now well-known "bubble" or localized region of laminar separated flow. He also distinguished between the leading-edge stalls characteristic of rounded and sharp-edged sections. The latter type of section, however, was dismissed as being impractical. Unfortunately, his experimental work was confined to force, pressure-distribution, and tuft observations so that direct correlation of the types of stall with boundary-layer flow was not possible.

In 1937, Jacobs and Sherman (reference 5) first related the type of flow separation to maximum-lift characteristics (and indirectly stalling) in a discussion of the effects of Reynolds number on the aerodynamic characteristics of airfoil sections. Although the type of stall characteristic of sharp-edged airfoils was not considered, Jacobs and Sherman described the importance of the laminar and turbulent boundary layer in the leading and trailing-edge types of stall. It is remarkable that the conclusions were reached without recourse to systematic measurements of the boundary layer. Recently (1948), Loftin and Bursnall (reference 6) extended the discussion of reference 5 on the basis of experimental data obtained since 1937, notably those of von Doenhoff and Tetervin (references 7 and 8). The importance of the localized region of laminar separated flow behind the leading edge in the effects of Reynolds number on the maximum lift of airfoil sections of various thicknesses is discussed by them at some length.

At the Ames Aeronautical Laboratory an investigation of the boundary-layer and stalling characteristics of the NACA 63_3-018 and 63_1-012 airfoil sections was undertaken to provide basic data for an application of boundary-layer control. The results of the boundary-layer-control investigation were published (references 9 and 10) and the preliminary investigations mentioned, but a complete presentation of the basic data was never made. The stalls of these two airfoils provided excellent examples of turbulent and laminar separation. As a direct approach to the stalling problem, the investigation was extended to include thinner airfoil sections (NACA 63-009, 64A006, and a sharp-edged section of 4.23-percent-thickness ratio). These results were published in references 11, 12, and 13. The latter studies were significant in that they provided the following information: The first history in which the bubble of laminar separation was traced from its first measurable appearance until it precipitated the stall; the observation of two types of separated flow originating near the leading edge of the same airfoil prior to the attainment of maximum lift; and the first known investigation of the details of the flow over a sharp-edged airfoil section at low angles of attack. Individually, these studies represent the investigations of particular airfoil sections, but collectively they cover a sufficiently wide range of thickness ratios to illustrate three general types of low-speed stalling characteristics observed under identical experimental

conditions. The three types of stalling characteristics are similar to those of Jones' original classification.

SOURCES OF DATA

The three types of stall and the associated separated flows will be described, and examples of each will be drawn from previously mentioned unpublished data for the NACA 63_3-018 and 63_1-012 airfoil sections as well as from references 11, 12, and 13. Descriptions of the airfoil models, apparatus, and techniques of the experimental investigations may be found in the references. Line drawings of the five airfoil sections are given in figure 1, and the coordinates of the four round-nosed sections are listed in table I. The plain flaps shown on three of the sections were not deflected for any of the tests mentioned herein. A typical installation in the wind tunnel of one of the models, all of which were of 5-foot chord, is shown in figure 2. Force and moment data[2] for the five airfoil sections are given in figures 3 and 4; representative pressure distributions[2] in figures 5 to 11; and boundary-layer data in figures 12 to 20. Pressure-distribution data from zero lift to beyond the stall for all the airfoil sections are tabulated in tables II to VI.

All data were obtained in the Ames 7- by 10-foot wind tunnels and, except those noted otherwise, were obtained for a Mach number of 0.17 and a Reynolds number of 5.8 million. The symbol notation is listed in appendix B.

DESCRIPTION OF THE THREE TYPES OF STALL

The three classifications of stalling will hereafter be designated as:

1. Trailing-edge stall (preceded by movement of the turbulent separation point forward from the trailing edge with increasing angle of attack)

2. Leading-edge stall (abrupt flow separation near the leading edge generally without subsequent reattachment)

---

[2]These data have not been corrected for tunnel-wall constraint or the effects of compressibility. The method of correction usually applied is described in reference 14. Numerical values of corrections to the force data are listed in appendix A.

3. Thin-airfoil stall (preceded by flow separation at the leading edge with reattachment at a point which moves progressively rearward with increasing angle of attack)

In the following paragraphs, those airfoil sections which fit uniquely into one of the preceding stalling classifications will be described first. Airfoil sections which combine two types of stall or those which possess borderline characteristics will be discussed later. The data on which the descriptions are based were obtained for a Reynolds number of 5,800,000. A change of Reynolds number or any of the factors which influence boundary-layer growth will affect stalling characteristics, and may cause the stall of a particular airfoil section to change from one classification to another.

Trailing-Edge Stall

This type of stall is characteristic of most thick airfoil sections (thickness ratios of approximately 0.15 and greater), and is probably better known than the two leading-edge types of stall. The example of trailing-edge stall was provided by the NACA 633-018 airfoil section. The force and moment characteristics (fig. 3) show smooth and continuous variations from zero lift to well beyond the stall. The peak of the lift curve is rounded, and the loss of lift as well as the increase of pressure drag after the stall is gradual. The variation of pitching moment with lift is smooth, and there is no sudden break at the stall. The profile drag (fig. 4) shows the characteristic range of low drag extending to an angle of attack of about 4°, followed by a relatively gradual increase of drag to the upper limit of the measurements.

The chordwise distribution of pressure (fig. 5) showed a progressive increase of the peak pressures near the leading edge with increasing angle of attack. The recovery of pressure over the rear portion of the airfoil was continuous for all angles of attack less than about 10°. For higher angles of attack the pressure failed to recover to the same degree as for the lower angles of attack and a region of nearly constant pressure, indicative of flow separation, appeared at the trailing edge. At maximum lift ($\alpha=14^{\circ}$) the pressure distribution was relatively flat over the rear half of the airfoil, but the peak pressures near the leading edge continued to increase after the stall.

Visual observation of tufts indicated that the flow remained attached to the upper surface of the model until an angle of attack of about 10° was attained. With further increase of angle of attack the flow began to separate from the rear of the airfoil, the extent of the separated region progressing steadily forward. At maximum lift the flow was separated over approximately the rear half of the airfoil. Beyond maximum lift the forward progression of separation continued at about the same rate as prior to the stall.

The development of the region of separated flow as indicated by the boundary-layer measurements was in good agreement with that shown by the pressure distributions and tuft studies. Previous investigations (e.g., references 15 and 16) have shown that the attainment of a value of 2.6 or 2.7 by the boundary-layer shape parameter H (see appendix B) is indicative that separation of the turbulent boundary layer has occurred. Extrapolation of the data in figure 12 shows that this value was first attained at the trailing edge for an angle of attack of about 10°. With further increase of angle of attack the separation point, as indicated by the shape parameter, moved progressively forward. For maximum lift, separation occurred between the 50- and 60-percent chord stations.

These data indicate that this type of stall results from turbulent separation moving progressively forward from the trailing edge with increasing angle of attack. The course of events which finally determines maximum lift begins well before maximum lift is attained. As soon as turbulent separation appears the lift-curve slope begins to decrease. As the chordwise extent of separation increases the lift-curve slope finally becomes zero and the airfoil is stalled. Throughout the range of moderate and large angles of attack the forward progression of separation and the changes of aerodynamic forces are gradual and continual.

Leading-Edge Stall

The leading-edge stall is generally inherent to most airfoil sections of moderate thickness (symmetrical sections with thickness ratios of approximately 0.09 to 0.15), and has become of general interest only comparatively recently. Examples of the leading-edge stall were furnished by the NACA 63_1-012 and 63-009 airfoil sections. The force and moment characteristics of these airfoil sections (fig. 3) show abrupt discontinuities when the angle of attack for maximum lift is exceeded. There is but little or no rounding over of the lift curves near maximum lift, and the peaks of the curves are sharp. Coincident with the loss of lift at the stall there is an abrupt increase of pressure drag and a negative shift of the pitching moment (the curve of which is relatively linear up to the stall). The profile drag (fig. 4) shows the low-drag range extending to an angle of attack of about 2° for the NACA 63_1-012 airfoil section and to slightly less than 2° for the NACA 63-009 airfoil section. The increase of drag outside the low-drag range is gradual for both sections within the limits of measurement. The force and moment discontinuities which accompanied the stall were less severe in the case of the NACA 63-009 airfoil section than for the NACA 63_1-012 airfoil section. Because of violent buffeting of the latter section when stalled, it was deemed unsafe to obtain data at the usual value of dynamic pressure; consequently all data points for angles of attack greater than that for maximum lift were obtained with the dynamic pressure reduced to correspond to a Reynolds number of 4,100,000.

The pressure distributions (figs. 6 and 7) show a continual increase of the peak negative pressures up to the angles of attack for maximum lift, followed by an abrupt collapse of the leading-edge pressure peaks. After the collapse of the pressure peaks, the static pressure was redistributed along the chord into the more or less flattened form characteristic of separated flow, which accounts for the negative shift of the pitching moment by virtue of the rearward shift of the center of pressure. In the case of the NACA 63-009 airfoil section (fig. 7), the region of nearly constant pressure extended to the 10-percent-chord station for an angle of attack of 9.0° ($c_{l_{max}}$ occurred for α=8.9°). Downstream of the flattened region there was considerable recovery of pressure, although the pressure did not recover to free-stream static pressure at the trailing edge. Further increases in the angle of attack increased the chordwise extent of the region of nearly constant pressure but reduced the magnitude of the negative pressure coefficients and the amount of pressure recovered at the trailing edge.

Tuft studies of the NACA 63_1-012 airfoil indicated that, up to the angle of attack for maximum lift (12.8°), smooth flow existed over the entire upper surface of the model. After the attainment of maximum lift, all the tufts appeared to indicate separation simultaneously and there was no evidence of flow reattachment at any station along the surface. As previously mentioned, the stall of this model was so violent that the tunnel speed was reduced immediately after the occurrence of the stall. Similar studies of the NACA 63-009 airfoil section also indicated smooth flow up to maximum lift (α=8.9°). Beyond the stall, the flow differed from that of the stalled NACA 63_1-012 airfoil. For an angle of attack of 9°, the tufts indicated separated or reversed flow from the leading edge to approximately 20-percent chord. Behind this region no definite pattern of separated flow was observed; the tufts always indicated flow in the downstream direction although the flow was exceedingly rough. This type of flow is similar to that described in the next section for the sharp-edged airfoil before the stall. Detailed investigation of the flow over the forward portion of the NACA 63-009 airfoil with a single-tuft probe and tufts attached to wires extending outward from the surface revealed that the reverse flow over the forward portion of the airfoil was part of a slow circulatory flow suggestive of a vortex centered above the airfoil surface at about 5-percent chord. Further increases in the angle of attack moved the apparent vortex center to a more rearward location and increased the chordwise extent of the reversed flow. It would appear, therefore, that up to the stall the NACA 63-009 airfoil falls into the leading-edge stall category, and after the stall assumes the type of flow which precedes the thin-airfoil stall.

The results of measurements of the turbulent boundary layer over the rear portions of the NACA 63_1-012 and 63-009 airfoils for angles up to the stall are presented in figures 13 and 14 as the chordwise variations of the derived parameters θ and H. In neither case did the shape parameter, even when extrapolated to the trailing edge, attain the

critical value of 2.6 which is indicative of the occurrence of turbulent separation. On the basis of these data it is apparent that the sudden stalls of the NACA 63_1-012 and 63-009 airfoil sections were not initiated by separation of the turbulent boundary layer which is a comparatively gradual process.

In order to study the flow conditions which preceded the sudden stall, the boundary layer near the leading edge of the NACA 63-009 airfoil was investigated both by direct measurement with small rakes and by the liquid-film method. A narrow region of separated flow near the leading edge was revealed by both methods. This small region or bubble was first discernible for an angle of attack of about 4°, and persisted up to the stall. The velocity profiles measured for angles of attack of 4° and 8° are presented in figure 15.[3] Also shown in the figures is the static pressure on the surface of the airfoil.

These data show that separation of the laminar boundary layer occurred near the leading edge prior to the stall, and that flow reattachment took place with a transitional-type boundary layer which changed to the turbulent type within a short distance downstream. Separation always occurred downstream of the pressure peak, and, characteristic of most separated-flow regions, a short extent of relatively constant surface pressure existed within the bubble, although pressure recovery began upstream of the point of flow reattachment.

The chordwise locations of the separation and reattachment points as determined by the boundary-layer surveys and by the liquid-film method are shown in figure 16. The correlation between the two methods is excellent considering the small extent of the region of separated flow. It is probable that the results of the liquid-film method, having the least interference effects, are the most reliable.

Attempts to define the separation bubble on the NACA 63_1-012 airfoil were unsuccessful because the rake was not moved forward in sufficiently small steps. However, the presence of a bubble similar to that on the NACA 63-009 airfoil was revealed by the liquid-film method.

---

[3]In the figure, the boundary-layer profiles are shown above the contour of the airfoil with the origins of the velocity axes (u/U) on the stations at which the profiles were measured. The y/c axes are normal to the surface, and for the sake of clarity, have been magnified 20 times with respect to the airfoil dimensions. The dashed portions of the profiles and the cross-hatched areas represent regions of reversed or separated flow. The fairing of the velocity profiles in this region is arbitrary because of the inability of the rake tubes immersed in the separated flow to indicate correctly the negative velocity of the flow.

The mechanism of the stall is, at present, considered to be attributable to the processes of separation and transition of the laminar boundary layer behind the leading-edge pressure peak. In the same manner as for the trailing-edge stall, the flow separation causing this type of stall begins well before the attainment of maximum lift, apparently shortly after the leading-edge pressure peak is formed. The laminar boundary layer passes around the leading edge, through the pressure peak, and separates. The subsequent processes, based on the speculation of von Doenhoff in reference 7, appear to be as follows: After separation, the detached laminar boundary layer continues away from the airfoil surface along a path approximately tangent to the surface at the point of separation. Transition then occurs and the expansion of the turbulent motion spreads at such an angle relative to the path of tangency of the separated laminar flow that the flow quickly reattaches to the surface as a turbulent boundary layer. This localized region of separated flow has become commonly known as the laminar-separation bubble. Increases in angle of attack move the pressure peak nearer the leading edge, and because the occurrence of laminar separation is primarily a function of pressure recovery, the point of laminar separation also moves forward. In addition, the extent of separated laminar flow is decreased, probably resulting from the decreased stability of the laminar boundary layer brought about by the greater adverse pressure gradient behind the pressure peak and the increased Reynolds number of the flow based on local conditions. As the point of separation moves forward, the separation and transition phenomenon takes place in a region of increasing curvature of the airfoil surface. Assuming, for the moment, that the length of separated laminar flow is fixed, any increase in local curvature would steadily move the transition point a greater distance above the airfoil surface, thereby rendering the process of the turbulent reattachment continually more difficult. However, such an apparent impairment of the reattachment of flow following transition is counteracted by the decrease in the length of the separated laminar run caused by the effect of angle-of-attack increase on the local Reynolds number and on the pressure gradient. Sufficient increase in angle of attack eventually moves the separation point so far forward that the flow does not reattach after transition occurs. Maximum lift has then been obtained. A complete disruption of the flow occurs over the entire upper surface and the aerodynamic forces, consequently, change abruptly in readjusting to the new flow about the airfoil section.

Thin-Airfoil Stall

The stall resulting from leading-edge separation with progressive rearward movement of the point of reattachment occurs on all sharp-edge airfoils and, as will be discussed later, apparently on some thin (thickness ratios of 0.09 and less) rounded-leading-edge airfoil sections. The example of this type of separation and stall is given by the thinnest of the five airfoils investigated, the double-wedge section modified to a thickness ratio of 0.0423.

The lift curve of the double-wedge airfoil section (fig. 3(a)) is linear to near maximum lift; the top of the curve is relatively flat and there is little loss of lift after the stall. The pressure drag (fig. 3(b)) shows a progressive and rapid increase starting at zero lift. The pitching moment (fig. 3(c)) shows a small positive trend for moderate lift coefficients followed by a pronounced negative trend near maximum lift. The profile drag (fig. 4) rises rapidly for angles of attack greater than 0.5°.

The pressure distribution (fig. 9) shows much lower pressure peaks near the leading edge than any of the round-nose airfoils. The failure to attain the high theoretical values of suction pressure over the forward portion of the airfoil accounts for the rapid increase of pressure drag shown in figure 3(b). As the angle of attack was increased from 0°, a region of essentially constant pressure formed immediately behind the leading edge and became of increasingly greater chordwise extent. For an angle of attack of 10° (1° beyond maximum lift), the pressure distribution was relatively flat along the entire upper surface. This variation of the pressure distribution accounts for the negative trend of the pitching moment.

Observation of tufts on the double-wedge airfoil indicated smooth flow for 0° angle of attack, but a localized region of separated flow near the leading edge appeared almost immediately upon increasing the angle of attack. Although the tufts downstream of the separated area indicated very rough flow, the flow became steadier as it approached the trailing edge. At higher angles of attack the chordwise extent of the separated region increased until it covered the entire upper surface of the model at the angle of attack for maximum lift. As the extent of this separated flow increased, an area of strong reverse flow, indicated by tufts pointing upstream, appeared in the region of separated flow. The injection of smoke into the region of separated flow revealed the presence of a circulatory motion in the flow above the upper surface of the model similar to that observed on the NACA 63-009 airfoil section after it had stalled.

The boundary-layer surveys on the double-wedge airfoil showed the presence of a variation in static pressure normal to the surface when the region of separated flow existed. The pressure first decreased and then increased with distance from the surface, the degree of variation being greatest in the region of separated flow and diminishing toward the trailing edge. Some velocity and static-pressure profiles are presented in figure 19. The usual boundary-layer parameters θ and H were not computed since the unusual shape of the velocity profiles and the presence of reverse flow cast doubt on the significance of these parameters. (Note that values of u/U greater than 1.0 were indicated.) The existence of strong reverse flow in the separated region in addition to the trend of the static-pressure profiles suggests that the separation from the leading edge results in the formation of a vortex motion as part

of the region of separated flow. Such a disturbance may account for the much greater thickness of the boundary layer for this type of airfoil as compared to those for the round-nose airfoil sections mentioned previously. The growth of the height and extent of the separated region (the boundary where $u/U=0$) is shown in figure 20. Although 3° is the smallest angle of attack for which data are shown in this figure, separated velocity profiles were measured for angles of attack of 1° and 2°.

The mechanism of the thin-airfoil stall is probably connected with the inability of the flow to remain attached to the surface while passing from the stagnation point around the sharp leading edge to the upper surface. The theoretically infinite (for an infinitely sharp edge) velocities are physically impossible and separation from the leading edge results as soon as stagnation moves to the lower surface. The separated flow passes above the surface of the airfoil and reattaches farther downstream. The exact mechanism of reattachment is, however, obscure. All that can be said, for the present, is that for low angles of attack the flow reattaches to the upper surface a short distance behind the leading edge and flows to the trailing edge without further separation. The boundary-layer velocity profile at the reattachment point does not resemble a typical laminar or a typical turbulent profile, but gradually adjusts itself into a fully developed turbulent boundary-layer profile before reaching the trailing edge. Increases in angle of attack move the point of reattachment toward the trailing edge. When the reattachment point coincides with the trailing edge (approximately) the stall is attained and further increases in angle of attack gradually reduce the lift and then increase it steadily to values greater than that at the stall. This second increase in lift occurs for angles of attack for which vortex streets have been measured in the wakes of flat plates (reference 17).

DISCUSSION

In the preceding description of the leading-edge and trailing-edge stalls, each type was treated as though it were totally independent of the other. Actually there is a mutual interaction between laminar and turbulent separation. Although not mentioned previously, a bubble of laminar separation developed on the NACA 63_3-018 airfoil section prior to the attainment of maximum lift. The presence of this bubble was not revealed by direct measurement but by plotting the pressure data for a given chordwise station against angle of attack. When a bubble passes over a pressure-measuring orifice the pressure will fail to change uniformly with angle of attack because of the region of relatively constant pressure within the bubble. Typical data showing this effect for each of the round-nose airfoils are presented in figure 11. In each case, including that of the 18-percent-thick airfoil, there is a small

discontinuity indicative of passage of a bubble over the pressure orifice.[4] The effect of this bubble of laminar separation on the initial thickness of the turbulent boundary layer has been noted by von Doenhoff and Tetervin (reference 8). For a given angle of attack the appearance of a laminar bubble, or an increase in the extent of an existing bubble, increases the initial thickness of the turbulent boundary layer and, hence, increases the tendency for the latter to separate. There can be little doubt that the laminar bubble tended to accelerate the turbulent stall of the NACA 633-018 airfoil section.

Through the medium of the circulation around an airfoil, the occurrence of turbulent separation also has an effect on laminar separation. For a given angle of attack the loss in circulation caused by turbulent separation reduces the local velocities over the airfoil which in turn increases the size of the bubble. This process favors earlier turbulent separation. However, the decrease in the pressure gradient along the airfoil, which accompanies the circulation decrease, tends to delay the occurrence of turbulent separation. As a result, the mutual interaction between the two types of boundary-layer separation is not a divergent process, and for most airfoils either laminar or turbulent flow separation is dominant.

There are some airfoil sections of intermediate thickness ratios to those stalling from predominantly laminar or turbulent separation which combine both types of flow separation. This situation has been described by B. M. Jones as a race between the two types of separation for the determination of maximum lift. In such cases either turbulent separation may move forward so rapidly that the lift curve has a relatively sharp peak, or a considerable extent of turbulent separated flow may form prior to complete laminar separation resulting in a rounding of the lift curve preceding the abrupt loss of lift which accompanies the leading-edge stall.

The pressure recovery prior to separation effected by the laminar boundary layer of the NACA 63-009 airfoil section was calculated by the theoretical method of von Kármán and Millikan (reference 18). The method employs two types of arbitrary velocity distributions termed "single-roof" and "double-roof" profiles, and predicts the value of the square of the ratio of the velocity at the separation point to the maximum velocity $(U_{sep}/U_{max})^2$. Use of the single-roof approximation gave a value of 0.81, and the double roof a value of 0.86 for all angles of attack.

---

[4]The second discontinuity in the curve for the NACA 63_1-012 airfoil is due to the effects of reduced Reynolds number and Mach number. The data points above the second discontinuity were obtained at a speed corresponding to a Reynolds number of 4.1 million and a Mach number of 0.12. The correction for the difference in Mach number amounts to about half the deviation from a continuous curve.

The experimental value was about 0.89 for all angles of attack for which separation was observed. Considering the rather crude approximation to the actual pressure distribution effected by the straight lines of the theoretical method, the agreement is good. These results emphasize that laminar separation near the leading edge is primarily dependent on the amount of pressure recovery the laminar boundary layer is capable of withstanding. The forward movement of the bubble of laminar separation with increasing angle of attack is, therefore, the result of the corresponding movement of the leading-edge pressure peak.

The length of the separated laminar run prior to transition, as mentioned previously, is undoubtedly dependent on the stability of the laminar flow. However, application of stability criteria to the problem of separated laminar flows near an airfoil leading edge has not yet been attempted. Further experimental and theoretical investigations are required.

A hypothesis advanced by von Doenhoff (reference 7) involved the simple relationship that the length of separated laminar flow prior to transition can be defined by a constant value of the Reynolds number based on the local velocity outside of the boundary layer at separation and the distance between the points of separation and the beginning of transition. According to this hypothesis, any increase in local velocity, whether due to increased angle of attack or increased free-stream velocity, would produce a decrease in the distance from separation to transition, and hence, in the extent of the bubble. With the assumption of a fixed angle of spread of turbulence, any reduction in the distance from separation to transition would tend to facilitate reattachment of the spreading turbulent flow. That increased Reynolds number does decrease the extent of the bubble of laminar separation was shown by the previously mentioned experiments of von Doenhoff and Tetervin (reference 8); the expected effects of angle-of-attack change were confirmed by the measurements made on the NACA 63-009 airfoil (reference 11). Moreover, this hypothesis has proved useful for explaining some effects of Reynolds number on maximum lift, and forms the basis for a large portion of the discussion by Loftin and Bursnall in reference 6. The value originally suggested for the Reynolds number of the separated laminar flow was 50,000. The values determined from boundary-layer measurements on the NACA 63-009 airfoil section vary from 60,000 for low values of lift coefficient to 30,000 near maximum lift. The liquid-film measurements, which should involve the least interference effects, give a value of about 60,000 for lift coefficients greater than 0.8. Thus, von Doenhoff's hypothesis appears to be a useful empirical relationship.

The large difference between the leading-edge and the thin-airfoil stalls, in spite of the fact that both are the result of flow separation from the leading edge, is emphasized by the flow characteristics observed for the NACA 64A006 airfoil section. For angles of attack up to 4.5° the

flow over this section was similar to that over the thicker round-nose sections, but between 4.5° and 5° the flow changed abruptly to a type similar to that observed for the double-wedge section. Compare, for example, the pressure distribution (figs. 8 and 9), the boundary-layer velocity and static-pressure profiles (figs. 17 and 19), and the general shape and growth of the region underlying the separated flow (figs. 18 and 20). For angles of attack as low as 3°, liquid-film observations and pressure-distribution measurements (figs. 10 and 11) revealed the presence of a bubble of laminar separation which persisted until the abrupt change in the nature of the flow. The latter was accompanied by discontinuities in the lift, drag, and pitching moment (fig. 3). Increasing the Reynolds number to 8.1 million delayed the abrupt change in flow to an angle of attack between 5° and 5.5°, a result which would be expected from the preceding discussion of the laminar bubble. It may be concluded, therefore, that the change in flow and the accompanying force and moment discontinuities were due to a separation of the laminar boundary layer similar to that which precipitated the stalls of the NACA 63_1-012 and 63-009 airfoil sections. The separated flow, instead of leaving the surface of the airfoil completely, assumed the characteristics of separated flow from a sharp-edged airfoil.

Since the flow for the stalled NACA 63-009 airfoil was remarkably similar to that observed for the double-wedge airfoil and for the NACA 64A006 airfoil for angles of attack greater than 4.5°, it appears that the occurrence of the flow separation which precipitates the leading-edge stall was, in these cases, succeeded by the thin-airfoil type of separated flow. The NACA 64A006 and to a lesser extent the NACA 63-009 airfoil sections represent cases which are on the borderline between airfoils subject solely to leading-edge or to thin-airfoil stalling. However, in contrast to the borderline case which combines laminar and turbulent separation, the leading-edge and thin-airfoil separated flows cannot occur simultaneously on the same airfoil section.

CONCLUDING REMARKS

Following the preceding sections in which the three types and combinations of separated flows and stalling characteristics were described, it is again desired to emphasize that every airfoil section cannot be classified uniquely into a given stalling category, nor is each type of stall limited to a given range of thickness ratios. Since stalling is inseparably related to the behavior of the boundary-layer flow, the same factors which influence boundary-layer growth (i.e., Reynolds number, stream turbulence, surface roughness, pressure gradient) also effect the stalling characteristics of airfoil sections. A change in any one of the factors may cause the stall of a given airfoil section to change from one type to another and variations in thickness distribution, leading-edge radius, and camber make it impossible to define

rigidly the thickness ratios applicable to each type. Although the analysis and illustrative examples of the three types of stall presented herein are based on a series of symmetrical airfoils investigated for one value of Reynolds number, it is believed that they illustrate the stalling characteristics of most practical airfoil sections.

Ames Aeronautical Laboratory,
National Advisory Committee for Aeronautics,
Moffett Field, Calif., July 23, 1951.

APPENDIX A

WIND-TUNNEL-WALL CORRECTIONS

The subscript u denotes the uncorrected coefficients presented in this report. The corrections were calculated by the method of reference 14. A minor correction based on the drag coefficient has been omitted.

NACA 63_3-018 Airfoil

$$\alpha = \alpha_u + 0.475\ c_{l_u} + 1.902\ c_{m_u}$$

$$c_l = 0.916\ c_{l_u}$$

$$c_d = 0.949\ c_{d_u}$$

$$c_m = 0.969\ c_{m_u} + 0.0132\ c_{l_u}$$

NACA 63_1-012 Airfoil

$$\alpha = \alpha_u + 0.475\ c_{l_u} + 1.902\ c_{m_u}$$

$$c_l = 0.926\ c_{l_u}$$

$$c_d = 0.968\ c_{d_u}$$

$$c_m = 0.979\ c_{m_u} + 0.0132\ c_{l_u}$$

NACA 63-009 Airfoil

$$\alpha = \alpha_u + 0.475\ c_{l_u} + 1.902\ c_{m_u}$$

$$c_l = 0.931\ c_{l_u}$$

$$c_d = 0.976\ c_{d_u}$$

$$c_m = 0.984\ c_{m_u} + 0.0132\ c_{l_u}$$

NACA 64A006 Airfoil

$$\alpha = \alpha_u + 0.475\ c_{l_u} + 1.902\ c_{m_u}$$

$$c_l = 0.936\ c_{l_u}$$

$$c_d = 0.983\ c_{d_u}$$

$$c_m = 0.989\ c_{m_u} + 0.0132\ c_{l_u}$$

Double-Wedge Airfoil

$$\alpha = \alpha_u + 0.475\ c_{l_u} + 1.902\ c_{m_u}$$

$$c_l = 0.941\ c_{l_u}$$

$$c_d = 0.993\ c_{d_u}$$

$$c_m = 0.994\ c_{m_u} + 0.0132\ c_{l_u}$$

APPENDIX B

NOTATION

The symbols used in this report are defined as follows:

c wing chord, feet

c_d section pressure-drag coefficient $\left(\frac{\text{pressure drag per unit span}}{qc}\right)$ as determined from integrated pressure-distribution diagrams

c_{d_o} section profile-drag coefficient $\left(\frac{D}{qc}\right)$ as determined from wake surveys

c_l section lift coefficient $\left(\frac{L}{qc}\right)$ as determined from integrated pressure-distribution diagrams

c_m section pitching-moment coefficient $\left(\frac{M}{qc^2}\right)$ as determined from integrated pressure-distribution diagrams

D drag per unit span, pounds

H boundary-layer shape parameter $\left(\frac{\delta^*}{\theta}\right)$

H_o free-stream total pressure, pounds per square foot

L lift per unit span, pounds

M pitching moment per unit span, pound-feet

p_l local static pressure on airfoil surface, pounds per square foot

p_o free-stream static pressure, pounds per square foot

P pressure coefficient $\left(\frac{p_l-p_o}{q}\right)$

q dynamic pressure (H_o-p_o), pounds per square foot

u local velocity within boundary layer, feet per second

U local velocity outside boundary layer, feet per second

x distance from airfoil leading edge measured parallel to chord line, feet

y distance above airfoil measured normal to surface, feet

α angle of attack, degrees

δ boundary-layer thickness, feet

δ^* boundary-layer displacement thickness $\left[\int_0^\delta \left(1 - \frac{u}{U}\right) dy\right]$, feet

θ boundary-layer momentum thickness $\left[\int_0^\delta \frac{u}{U}\left(1 - \frac{u}{U}\right) dy\right]$, feet

REFERENCES

1. Jacobs, Eastman N.: The Aerodynamic Characteristics of Eight Very Thick Airfoils from Tests in the Variable Density Wind Tunnel. NACA Rep. 391, 1931.

2. Millikan, C. B., and Klein, A. L.: The Effect of Turbulence. Aircraft Engineering, vol. 5, no. 8, August, 1933, pp. 169–174.

3. Jones, B. Melvill: An Experimental Study of the Stalling of Wings. R.&M. No. 1588, British A.R.C., 1933.

4. Jones, B. Melvill: Stalling. Jour. Royal Aero. Soc., vol. 38, no. 285, Sept. 1934, pp. 753–770. (22d Wilbur Wright Memorial Lecture.)

5. Jacobs, Eastman N., and Sherman, Albert: Airfoil Section Characteristics as Affected by Variations of the Reynolds Number. NACA Rep. 586, 1937.

6. Loftin, Laurence K., and Bursnall, William J.: The Effects of Variations in Reynolds Number Between 3.0×10^6 and 25.0×10^6 Upon the Aerodynamic Characteristics of a Number of NACA 6-Series Airfoil Sections. NACA TN 1773, 1948.

7. von Doenhoff, Albert E.: A Preliminary Investigation of Boundary-Layer Transition Along a Flat Plate with Adverse Pressure Gradient. NACA TN 639, 1938.

8. von Doenhoff, Albert E., and Tetervin, Neal: Investigation of the Variation of Lift Coefficient with Reynolds Number at a Moderate Angle of Attack on a Low-Drag Airfoil. NACA CB(19), November 1942.

9. McCullough, George B., and Gault, Donald E.: An Experimental Investigation of the NACA 63_1-012 Airfoil Section With Leading-Edge Suction Slots. NACA TN 1683, 1948.

10. McCullough, George B., and Gault, Donald E.: An Experimental Investigation of the NACA 63_1-012 Airfoil Section With Leading-Edge and Midchord Suction Slots. NACA TN 2041, 1950.

11. Gault, Donald E.: Boundary-Layer and Stalling Characteristics of the NACA 63-009 Airfoil Section. NACA TN 1894, 1949.

12. McCullough, George B., and Gault, Donald E.: Boundary-Layer and Stalling Characteristics of the NACA 64A006 Airfoil Section. NACA TN 1923, 1949.

13. Rose, Leonard M., and Altman, John M.: Low-Speed Investigation of the Stalling of a Thin, Faired, Double-Wedge Airfoil With Nose Flap. NACA TN 2172, 1950.

14. Allen, H. Julian, and Vincenti, Walter G.: Wall Interference in a Two-Dimensional-Flow Wind Tunnel, with Consideration of the Effect of Compressibility. NACA Rep. 782, 1944. (Formerly ARR 4K03)

15. von Doenhoff, Albert E., and Tetervin, Neal: Determination of General Relations for the Behavior of the Turbulent Boundary Layers. NACA Rep. 772, 1943. (Formerly NACA ACR 3G13)

16. Schubauer, G. B., and Klebanoff, P. S.: Investigation of Separation of the Turbulent Boundary Layer. NACA TN 2133, 1950.

17. Fage, A., and Johansen, F. C.: On the Flow of Air Behind an Inclined Flat Plate of Infinite Span. R.&M. No. 1104, British A.R.C., 1927.

18. von Karman, Th., and Millikan, C. B.: On the Theory of Laminar Boundary Layers Involving Separation. NACA Rep. No. 504, 1934.

TABLE I

COORDINATES OF THE AIRFOIL SECTIONS

Station (percent chord)	NACA airfoil section ordinate (percent chord)			
	63_3-018	63_1-012	63-009	64A006
0	0	0	0	0
.5	1.404	.985	.749	.485
.75	1.713	1.194	.906	.585
1.25	2.217	1.519	1.151	.739
2.50	3.104	2.102	1.582	1.016
5.0	4.362	2.925	2.196	1.399
7.5	5.308	3.542	2.655	1.684
10.0	6.068	4.039	3.024	1.919
15	7.225	4.799	3.591	2.283
20	8.048	5.342	3.997	2.557
25	8.600	5.712	4.275	2.757
30	8.913	5.930	4.442	2.896
35	9.000	6.000	4.500	2.977
40	8.845	5.920	4.447	2.999
45	8.482	5.704	4.296	2.945
50	7.942	5.370	4.056	2.825
55	7.256	4.935	3.739	2.653
60	6.455	4.420	3.358	2.438
65	5.567	3.840	2.928	2.188
70	4.622	3.210	2.458	1.907
75	3.650	2.556	1.966	1.602
80	2.691	1.902	1.471	1.285
85	1.787	1.274	.990	.967
90	.985	.707	.550	.649
95	.348	.250	.196	.331
100	0	0	0	.013
L.E. radius (percent chord)	2.120	1.087	.631	.246
T.E. radius (percent chord)	- - -	- - -	- - -	.041

TABLE II.– PRESSURE DISTRIBUTION FOR THE NACA 63_3–018 AIRFOIL SECTION

	PRESSURE COEFFICIENT, P																			
Angle of Attack, α	0°		1°		2°		3°		4°		5°		6°		7°		8°		9°	
Chordwise Station (Percent chord)	Upper	Lower	Upper	Lower	Upper	Lower	Upper	Lower	Upper	Lower	Upper	Lower	Upper	Lower	Upper	Lower	Upper	Lower	Upper	Lower
0	0.994	---	0.974	---	0.884	---	0.684	---	0.421	---	0.099	---	-0.290	---	-0.760	---	-1.296	---	-1.884	---
.37	.599	0.580	.359	0.769	.032	0.910	-.335	0.981	-.763	1.000	-1.225	0.954	-1.760	0.871	-2.350	0.721	-2.995	0.520	-3.658	0.271
1.25	.217	.185	-.032	.397	-.342	.606	-.665	.761	-1.026	.868	-1.397	.940	-1.820	.987	-2.285	1.007	-2.775	.987	-3.250	.936
2.50	-.038	-.070	-.256	.128	-.529	.335	-.800	.503	-1.105	.644	-1.404	.748	-1.740	.845	-2.102	.916	-2.488	.974	-2.878	1.000
5	-.287	-.287	-.449	-.115	-.658	.071	-.865	.232	-1.092	.369	-1.311	.477	-1.565	.600	-1.845	.688	-2.066	.770	-2.335	.846
7.50	-.395	-.420	-.551	-.263	-.742	-.097	-.916	.052	-1.112	.184	-1.298	.292	-1.510	.406	-1.708	.506	-1.934	.592	-2.142	.678
10	-.433	-.446	-.570	-.308	-.729	-.161	-.884	-.026	-1.046	.092	-1.193	.199	-1.348	.303	-1.545	.396	-1.737	.487	-1.904	.574
15	-.529	-.541	-.641	-.423	-.781	-.297	-.897	-.181	-1.033	-.069	-1.146	.020	-1.234	.120	-1.435	.208	-1.585	.290	-1.710	.368
20	-.560	-.573	-.667	-.474	-.781	-.368	-.884	-.258	-1.000	-.171	-1.080	-.086	-1.200	.013	-1.325	.084	-1.447	.158	-1.555	.239
25	-.624	-.637	-.718	-.545	-.813	-.445	-.903	-.348	-.994	-.263	-1.073	-.185	-1.180	-.103	-1.285	-.026	-1.394	.039	-1.465	.116
30	-.624	-.624	-.705	-.545	-.787	-.458	-.865	-.368	-.934	-.290	-1.014	-.225	-1.103	-.148	-1.195	-.084	-1.276	-.013	-1.335	.058
35	-.624	-.624	-.692	-.558	-.768	-.477	-.826	-.400	-.901	-.329	-.967	-.258	-1.038	-.194	-1.117	-.136	-1.190	-.079	-1.238	-.001
40	-.592	-.592	-.654	-.532	-.729	-.438	-.761	-.387	-.836	-.323	-.888	-.265	-.948	-.207	-1.013	-.149	-1.073	-.099	-1.109	-.039
45	-.548	-.541	-.590	-.481	-.619	-.419	-.677	-.348	-.737	-.303	-.782	-.245	-.832	-.187	-.883	-.143	-.934	-.099	-.955	-.045
50	-.420	-.420	-.474	-.372	-.583	-.335	-.568	-.297	-.618	-.250	-.649	-.199	-.690	-.148	-.740	-.117	-.776	-.079	-.734	-.019
55	-.357	-.376	-.404	-.333	-.439	-.290	-.477	-.239	-.513	-.198	-.543	-.179	-.574	-.136	-.610	-.097	-.638	-.066	-.652	-.019
60	-.267	-.248	-.301	-.218	-.323	-.174	-.355	-.135	-.382	-.105	-.411	-.066	-.432	-.026	-.468	-.013	-.487	-.059	-.490	.039
65	-.191	-.178	-.218	-.147	-.239	-.110	-.258	-.077	-.290	-.053	-.305	-.027	-.323	.006	-.344	.026	-.355	.059	-.361	.090
70	-.102	-.127	-.128	-.103	-.148	-.071	-.161	-.045	-.184	-.026	-.199	.007	-.213	.103	-.234	.052	-.244	.086	-.239	.108
75	-.057	-.064	-.077	-.051	-.090	-.019	-.103	0	-.118	.020	-.138	.040	-.136	.065	-.149	.078	-.158	.099	-.148	.123
80	.038	.025	.019	.038	.006	.058	0	.077	-.013	.086	-.027	.106	-.032	.136	-.045	.143	-.059	.158	-.058	.174
85	.102	.096	.090	.103	.084	.123	.077	.142	.066	.151	.053	.159	.045	.181	.026	.182	0	.197	.001	.213
90	.166	.152	.154	.154	.148	.174	.142	.181	.132	.191	.119	.199	.110	.213	.091	.214	.079	.224	.071	.239
95	.229	.204	.218	.212	.226	.219	.206	.232	.197	.237	.179	.239	.174	.252	.149	.247	.132	.250	.110	.258

	PRESSURE COEFFICIENT, P																	
Angle of Attack, α	10°		11°		12°		13°		14°		15°		16°		17°		18°	
Chordwise Station (Percent chord)	Upper	Lower	Upper	Lower	Upper	Lower	Upper	Lower	Upper	Lower	Upper	Lower	Upper	Lower	Upper	Lower	Upper	Lower
0	-2.512	---	-3.130	---	-3.764	---	-4.367	---	-4.780	---	-4.940	---	-5.145	---	-5.442	---	-5.571	---
.37	-4.365	-0.013	-5.006	-0.318	-5.355	-0.637	-6.019	-0.943	-6.484	-1.156	-6.443	-1.258	-6.592	-1.396	-6.848	-1.537	-7.048	-1.640
1.25	-3.780	.859	-4.250	.766	-4.758	.656	-5.247	.544	-5.510	.474	-5.410	.424	-5.270	.358	-5.375	.443	-5.434	.267
2.50	-3.172	1.006	-3.505	.994	-3.860	.974	-4.164	.937	-4.375	.935	-4.382	.914	-4.409	.886	-4.518	.879	-4.515	.850
5	-2.615	.891	-2.838	.929	-3.063	.962	-3.266	.981	-3.390	1.000	-3.363	.993	-3.340	.994	-3.385	1.000	-3.348	1.000
7.50	-2.378	.744	-2.540	.798	-2.720	.847	-2.873	.880	-2.955	.909	-2.900	.914	-2.860	.918	-2.880	.933	-2.807	.935
10	-2.095	.628	-2.232	.695	-2.248	.745	-2.494	.778	-2.552	.812	-2.483	.821	-2.420	.830	-2.425	.846	-2.338	.850
15	-1.852	.436	-1.955	.500	-2.051	.554	-2.127	.595	-2.142	.623	-2.052	.636	-1.962	.647	-1.913	.664	-1.790	.667
20	-1.666	.301	-1.746	.370	-1.822	.414	-1.861	.456	-1.856	.481	-1.728	.490	-1.585	.503	-1.500	.510	-1.360	.518
25	-1.564	.173	-1.615	.240	-1.675	.287	-1.703	.323	-1.649	.338	-1.490	.344	-1.314	.358	-1.181	.369	-.969	.361
30	-1.423	.109	-1.460	.169	-1.503	.210	-1.506	.247	-1.415	.260	-1.193	.258	-.974	.271	-.812	.275	-.649	.270
35	-1.307	.038	-1.337	.097	-1.357	.140	-1.342	.165	-1.195	.182	-.901	.172	-.654	.182	-.570	.181	-.538	.172
40	-1.166	.006	-1.182	.058	-1.191	.096	-1.139	.120	-.935	.130	-.623	.119	-.478	.126	-.483	.114	-.512	.100
45	-1.000	0	-1.007	.045	-1.000	.070	-.924	.095	-.675	.091	-.477	.079	-.421	.082	-.463	.074	-.512	.055
50	-.827	.013	-.825	.032	-.809	.083	-.703	.095	-.493	.091	-.424	.079	-.421	.069	-.477	.054	-.519	.035
55	-.673	.013	-.662	.032	-.631	.070	-.513	.082	-.422	.078	-.431	.053	-.428	.044	-.481	.027	-.525	-.004
60	-.506	.064	-.494	.097	-.489	.108	-.373	.120	-.403	.110	-.431	.086	-.446	.075	-.499	.047	-.551	.022
65	-.372	.109	-.351	.136	-.318	.146	-.297	.139	-.403	.130	-.464	.093	-.465	.082	-.517	.040	-.565	.009
70	-.244	.128	-.227	.156	-.210	.172	-.259	.177	-.403	.156	-.470	.119	-.478	.107	-.524	.054	-.578	.022
75	-.160	.141	-.149	.196	-.146	.159	-.228	.152	-.390	.130	-.464	.099	-.484	.082	-.530	.056	-.584	.022
80	-.077	.179	-.078	.188	-.108	.197	-.203	.190	-.370	.156	-.464	.119	-.484	.094	-.530	.067	-.584	.029
85	-.013	.218	-.019	.227	-.070	.223	-.177	.203	-.351	.169	-.450	.119	-.472	.094	-.523	.060	-.578	.022
90	.038	.231	.019	.240	-.045	.236	-.152	.203	-.312	.156	-.437	.099	-.453	.069	-.510	.034	-.565	-.004
95	.083	.250	.045	.253	-.013	.242	-.127	.203	-.279	.136	-.391	.073	-.421	.038	-.483	0	-.532	-.043

NACA

TABLE III.– PRESSURE DISTRIBUTION FOR THE NACA 63_1-012 AIRFOIL SECTION

	PRESSURE COEFFICIENT, P															
Angle of Attack, α	-0.2°		0.8°		1.8°		2.8°		3.8°		4.8°		5.8°		6.8°	
Chordwise Station (Percent chord)	Upper	Lower	Upper	Lower	Upper	Lower	Upper	Lower	Upper	Lower	Upper	Lower	Upper	Lower	Upper	Lower
0	1.000	---	0.940	---	0.745	---	0.410	---	-0.087	---	-0.688	---	-1.450	---	-2.353	---
.33	.405	0.290	.005	0.621	-.449	0.847	-.960	0.965	-1.602	1.000	-2.850	0.960	-3.040	0.838	-3.970	0.636
1.25	.080	.015	-.253	.268	-.561	.500	-1.010	.690	-1.475	.847	-1.859	.930	-2.485	.890	-3.242	1.000
2.50	-.060	-.185	-.334	.066	-.612	.281	-.900	.460	-1.275	.622	-1.533	.738	-1.855	.859	-2.292	.935
5	-.190	-.260	-.394	-.071	-.612	.092	-.880	.240	-.980	.383	-1.241	.497	-1.475	.616	-1.777	.712
7.50	-.240	-.300	-.404	-.136	-.582	0	-.740	.130	-.903	.260	-1.080	.362	-1.273	.470	-1.510	.571
10	-.270	-.325	-.424	-.182	-.556	-.061	-.700	.055	-.852	.168	-1.000	.271	-1.162	.379	-1.353	.460
15	-.300	-.350	-.429	-.237	-.546	-.168	-.640	-.035	-.765	.061	-.864	.146	-1.010	.252	-1.197	.313
20	-.345	-.395	-.440	-.298	-.546	-.209	-.635	-.110	-.734	-.036	-.839	.050	-.919	.126	-1.056	.212
25	-.345	-.385	-.439	-.303	-.526	-.235	-.600	-.150	-.694	-.066	-.779	0	-.848	.066	-.955	.142
30	-.370	-.395	-.450	-.333	-.510	-.260	-.565	-.185	-.661	-.117	-.729	-.080	-.813	.010	-.894	.076
35	-.380	-.395	-.450	-.338	-.500	-.270	-.565	-.200	-.643	-.143	-.694	-.080	-.798	-.040	-.828	.030
40	-.360	-.380	-.424	-.313	-.465	-.270	-.525	-.210	-.598	-.158	-.628	-.101	-.687	-.056	-.758	0
45	-.320	-.350	-.364	-.298	-.413	-.240	-.460	-.185	-.526	-.143	-.553	-.085	-.606	-.095	-.667	0
50	-.265	-.280	-.303	-.247	-.352	-.209	-.390	-.170	-.439	-.128	-.473	-.085	-.520	-.040	-.566	.005
55	-.230	-.250	-.273	-.202	-.311	-.184	-.345	-.150	-.388	-.107	-.418	-.070	-.450	-.040	-.495	.005
60	-.180	-.200	-.207	-.172	-.250	-.138	-.285	-.099	-.311	-.077	-.337	-.040	-.364	-.015	-.389	.025
65	-.160	-.150	-.192	-.121	-.214	-.092	-.235	-.070	-.265	-.036	-.276	0	-.303	.020	-.323	.050
70	-.075	-.080	-.101	-.071	-.123	-.051	-.140	-.035	-.168	-.010	-.176	.020	-.192	.040	-.218	.071
75	-.035	-.050	-.060	-.010	-.082	0	-.100	.020	-.117	.041	-.131	.070	-.152	.091	-.167	.111
80	.015	0	-.010	.020	-.026	.041	-.040	.050	-.051	.082	-.075	.101	-.091	.106	-.101	.126
85	.075	.060	.060	.071	.041	.087	.025	.100	.015	.112	0	.126	-.005	.141	-.025	.157
90	.110	.105	.101	.102	.087	.128	.060	.140	.061	.143	.050	.161	.050	.162	.035	.177
95.90	.160	.155	.141	.162	.143	.173	.135	.175	.123	.179	.116	.186	.111	.192	.101	.202

	PRESSURE COEFFICIENT, P															
Angle of Attack, α	7.8°		8.8°		9.8°		10.8°		11.8°		12.3°		12.8°		13.8°	
Chordwise Station (Percent chord)	Upper	Lower	Upper	Lower	Upper	Lower	Upper	Lower	Upper	Lower	Upper	Lower	Upper	Lower	Upper	Lower
0	-3.310	---	-4.441	---	-5.710	---	-6.850	---	-8.040	---	-8.870	---	-9.570	---	-1.427	---
.33	-4.830	0.366	-5.805	-0.010	-6.779	-0.425	-7.790	-0.909	-8.810	-1.426	-9.600	-1.716	-10.830	-1.915	-1.525	0.612
1.25	-3.360	.985	-4.081	.905	-4.817	.817	-5.540	.696	-6.850	.553	-6.280	.455	-6.630	.383	-1.376	.983
2.50	-2.660	.980	-3.073	.990	-3.524	1.000	-3.979	.984	-4.920	.959	-4.635	.924	-4.725	.895	-1.333	.966
5	-2.015	.792	-2.290	.840	-2.585	.900	-2.868	.944	-3.150	.984	-3.291	.984	-3.338	.990	-1.308	.795
7.50	-1.685	.640	-1.894	.704	-2.125	.780	-2.348	.833	-2.552	.888	-2.658	.899	-2.688	.915	-1.291	.658
10	-1.318	.538	-1.674	.605	-1.874	.680	-2.050	.742	-2.211	.795	-2.302	.808	-2.328	.830	-1.274	.538
15	-1.270	.386	-1.400	.450	-1.544	.525	-1.675	.581	-1.800	.640	-1.858	.656	-1.870	.676	-1.271	.376
20	-1.147	.264	-1.240	.340	-1.375	.395	-1.464	.464	-1.578	.518	-1.605	.530	-1.621	.547	-1.188	.265
25	-1.040	.188	-1.120	.250	-1.215	.310	-1.303	.363	-1.375	.411	-1.414	.439	-1.428	.428	-1.154	.162
30	-.960	.127	-1.010	.200	-1.115	.245	-1.186	.298	-1.244	.350	-1.277	.364	-1.279	.378	-1.128	.077
35	-.895	.035	-.945	.140	-1.015	.185	-1.073	.237	-1.122	.279	-1.158	.313	-1.155	.304	-1.085	.026
40	-.802	.046	-.845	.100	-.905	.145	-.960	.202	-.995	.228	-1.015	.272	-1.015	.268	-1.051	-.043
45	-.706	.025	-.735	.090	-.785	.195	-.823	.177	-.863	.208	-.874	.237	-.866	.239	-1.017	-.077
50	-.599	.036	-.620	.090	-.673	.115	-.702	.162	-.716	.198	-.732	.227	-.726	.219	-.983	-.094
55	-.528	.036	-.510	.080	-.580	.110	-.596	.146	-.614	.178	-.621	.197	-.617	.209	-.949	-.094
60	-.411	.046	-.420	.090	-.469	.115	-.429	.146	-.487	.168	-.495	.197	-.493	.194	-.897	-.103
65	-.335	.076	-.350	.100	-.375	.130	-.394	.152	-.386	.178	-.389	.202	-.378	.199	-.880	-.111
70	-.228	.076	-.230	.100	-.265	.130	-.278	.131	-.274	.168	-.278	.177	-.274	.184	-.846	-.111
75	-.178	.127	-.180	.150	-.190	.170	-.202	.182	-.203	.203	-.202	.213	-.199	.219	-.812	-.094
80	-.102	.142	-.110	.160	-.115	.175	-.126	.192	-.127	.203	-.126	.213	-.129	.209	-.778	-.103
85	-.041	.173	-.030	.190	-.035	.200	-.051	.212	-.061	.218	-.061	.229	-.065	.219	-.726	-.111
90	.035	.188	.025	.200	.015	.210	0	.212	-.010	.218	-.010	.229	-.020	.229	-.684	-.120
95.90	.086	.203	.090	.215	.075	.210	.061	.212	.041	.218	.036	.213	.025	.209	-.624	-.222

	PRESSURE COEFFICIENT, P															
Angle of Attack, α	14.8°		15.8°		16.8°		17.8°		18.8°		19.8°		20.8°		21.8°	
Chordwise Station (Percent chord)	Upper	Lower	Upper	Lower	Upper	Lower	Upper	Lower	Upper	Lower	Upper	Lower	Upper	Lower	Upper	Lower
0.	-1.034	---	-0.915	---	-0.861	---	-0.867	---	-0.932	---	-0.983	---	-1.078	---	-1.118	---
.33	-1.130	0.598	-.987	0.742	-.910	0.720	-.878	0.690	-.923	0.674	-.937	0.600	-.990	0.500	-1.012	0.450
1.25	-1.060	.983	-.949	.992	-.877	.984	-.898	1.000	-.881	.983	-.897	.983	-.948	.983	-.966	.948
2.50	-1.034	.932	-.932	.949	-.892	.943	-.842	.996	-.864	.966	-.889	.966	-.930	1.000	-.948	.991
5	-1.026	.781	-.915	.763	-.892	.752	-.833	.783	-.864	.805	-.880	.829	-.930	.861	-.948	.862
7.50	-1.017	.624	-.924	.627	-.892	.631	-.842	.650	-.864	.678	-.889	.701	-.930	.739	-.948	.741
10	-1.017	.504	-.924	.500	-.861	.500	-.842	.533	-.873	.551	-.889	.573	-.930	.617	-.948	.638
15	-1.000	.350	-.924	.339	-.869	.344	-.850	.367	-.881	.390	-.897	.419	-.939	.443	-.966	.466
20	-.991	.231	-.932	.220	-.877	.230	-.850	.250	-.881	.274	-.897	.282	-.948	.322	-.966	.345
25	-.991	.128	-.932	.110	-.885	.115	-.867	.133	-.898	.144	-.915	.162	-.957	.200	-.983	.207
30	-.991	.043	-.949	.025	-.893	.016	-.883	.042	-.907	.051	-.923	.068	-.965	.096	-.983	.103
35	-.966	-.009	-.949	-.034	-.910	-.033	-.883	-.025	-.915	-.017	-.932	0	-.974	.026	-1.000	.034
40	-.966	-.077	-.949	-.110	-.918	-.115	-.892	-.100	-.924	-.102	-.932	-.085	-.983	-.061	-1.000	-.060
45	-.966	-.111	-.958	-.153	-.918	-.164	-.900	-.150	-.932	-.153	-.949	-.137	-.983	-.130	-1.017	.121
50	-.966	-.145	-.966	-.169	-.934	-.180	-.917	-.183	-.949	-.186	-.949	-.179	-1.000	-.165	-1.017	.178
55	-.949	-.145	-.966	-.186	-.934	-.197	-.917	-.200	-.949	-.203	-.957	-.197	-1.000	-.191	-1.026	.190
60	-.949	-.162	-.966	-.203	-.934	-.213	-.933	-.217	-.949	-.237	-.966	-.231	-1.009	-.226	-1.026	.224
65	-.932	-.162	-.966	-.203	-.951	-.230	-.925	-.225	-.966	-.237	-.966	-.248	-1.009	-.235	-1.026	.250
70	-.915	-.162	-.966	-.212	-.951	-.238	-.925	-.250	-.966	-.254	-.966	-.265	-1.009	-.270	-1.034	.276
75	-.897	-.162	-.958	-.212	-.951	-.238	-.925	-.250	-.966	-.263	-.966	-.265	-1.017	-.270	-1.034	.293
80	-.872	-.171	-.932	-.220	-.934	-.246	-.917	-.258	-.949	-.280	-.966	-.282	-1.000	-.304	-1.034	.310
85	-.829	-.179	-.907	-.237	-.918	-.262	-.900	-.267	-.932	-.305	-.949	-.299	-.991	-.322	-1.017	.345
90	-.799	-.179	-.864	-.246	-.885	-.279	-.892	-.300	-.915	-.322	-.932	-.333	-.983	-.357	-1.000	.379
95.90	-.725	-.299	-.814	-.372	-.836	-.410	-.850	-.433	-.881	-.458	-.915	-.470	-.957	-.513	-.983	.534

TABLE IV.– PRESSURE DISTRIBUTION FOR THE NACA 63-009 AIRFOIL SECTION

	PRESSURE COEFFICIENT, P													
Angle of Attack, α	0°		1°		2°		3°		4°		5°		6°	
Chordwise Station (Percent chord)	Upper	Lower	Upper	Lower	Upper	Lower	Upper	Lower	Upper	Lower	Upper	Lower	Upper	Lower
0	1.000	- - -	0.924	- - -	0.645	- - -	0.150	- - -	-0.603	- - -	-1.509	- - -	-2.673	- - -
.1	.707	0.692	.283	0.934	-.305	1.000	-1.104	0.910	-2.145	0.624	-3.299	0.177	-4.682	-0.472
.25	.364	.394	-.131	.727	-.746	.934	-1.524	1.000	-2.489	.905	-3.515	.778	-4.715	.452
.5	.131	.141	-.318	.495	-.853	.762	-1.504	.930	-2.286	1.000	-3.122	.980	-4.155	.869
.75	.020	.040	-.394	.379	-.879	.645	-1.450	.845	-2.135	.965	-2.890	1.000	-3.820	.995
1.25	-.056	-.076	-.404	.232	-.792	.477	-1.249	.680	-1.849	.835	-2.004	.939	-2.622	.990
2.5	-.121	-.106	-.374	.116	-.645	.320	-.965	.495	-1.256	.639	-1.591	.763	-1.974	.859
5	-.182	-.162	-.359	.010	-.548	.168	-.745	.305	-.990	.437	-1.207	.556	-1.458	.653
7.5	-.222	-.212	-.369	-.066	-.518	.071	-.695	.190	-.885	.312	-1.056	.419	-1.252	.518
10	-.242	-.222	-.364	-.096	-.487	.025	-.635	.135	-.799	.236	-.944	.344	-1.111	.432
15	-.242	-.232	-.338	-.136	-.437	-.030	-.560	.055	-.689	.146	-.798	.232	-.925	.312
20	-.253	-.243	-.338	-.157	-.416	-.076	-.520	.005	-.688	.080	-.722	.167	-.824	.231
25	-.263	-.263	-.333	-.182	-.401	-.102	-.485	-.030	-.578	.035	-.657	.106	-.744	.171
30	-.268	-.263	-.328	-.192	-.391	-.122	-.470	-.060	-.553	0	-.621	.066	-.698	.126
35	-.278	-.263	-.344	-.207	-.391	-.137	-.460	-.080	-.528	-.025	-.591	.035	-.653	.085
40	-.263	-.258	-.318	-.207	-.366	-.147	-.425	-.100	-.488	-.040	-.540	.010	-.593	.060
45	-.237	-.237	-.278	-.192	-.325	-.132	-.375	-.090	-.432	-.040	-.475	.005	-.523	.050
50	-.212	-.207	-.253	-.172	-.295	-.122	-.340	-.080	-.382	-.035	-.424	.010	-.468	.050
55	-.177	-.167	-.227	-.151	-.254	-.107	-.295	-.065	-.332	-.025	-.369	.010	-.402	.050
60	-.136	-.131	-.182	-.091	-.208	-.071	-.240	-.045	-.276	-.005	-.308	.030	-.332	.060
65	-.091	-.101	-.131	-.076	-.152	-.036	-.185	-.015	-.211	.010	-.237	.040	-.261	.070
70	-.061	-.066	-.086	-.045	-.112	-.015	-.135	.015	-.161	.040	-.177	.051	-.201	.080
75	-.015	-.040	-.040	-.015	-.056	.005	-.080	.035	-.101	.055	-.116	.081	-.136	.096
80	.020	0	0	.025	-.015	.041	-.025	.065	-.045	.080	-.056	.106	-.075	.121
85	.051	.035	.040	.061	.030	.071	.020	.090	0	.101	-.005	.126	-.025	.136
90	.116	.096	.101	.101	.081	.107	.070	.125	.055	.131	.051	.146	.040	.156
95	.136	.111	.126	.136	.122	.137	.105	.140	.096	.156	.096	.157	.085	.166

	PRESSURE COEFFICIENT, P											
Angle of Attack, α	7°		8°		8.5°		8.9°		9°		10°	
Chordwise Station (Percent chord)	Upper	Lower	Upper	Lower	Upper	Lower	Upper	Lower	Upper	Lower	Upper	Lower
0	-4.055	- - -	-5.562	- - -	-6.370	- - -	-7.120	- - -	-1.622	- - -	-1.533	- - -
.1	-6.298	-1.273	-7.978	-2.213	-8.860	-2.738	-9.710	-3.191	-1.797	-.263	-1.523	-.152
.25	-6.080	.010	-7.458	-.531	-8.190	-.798	-8.938	-1.118	-1.758	.465	-1.492	.513
.5	-5.490	.634	-6.430	.413	-6.610	.237	-6.920	.108	-1.773	.848	-1.502	.853
.75	-4.215	.908	-5.099	.766	-5.550	.661	-6.001	.593	-1.737	.960	-1.482	.965
1.25	-3.298	1.000	-3.908	.979	-4.216	.934	-4.524	.918	-1.717	1.000	-1.456	.995
2.5	-2.555	.943	-2.781	.989	-2.990	.995	-3.180	1.000	-1.706	.934	-1.401	.914
5	-1.821	.753	-1.969	.832	-2.100	.854	-2.238	.887	-1.747	.758	-1.472	.741
7.5	-1.464	.613	-1.653	.694	-1.757	.722	-1.856	.758	-1.767	.626	-1.502	.619
10	-1.278	.516	-1.443	.597	-1.525	.626	-1.613	.655	-1.757	.535	-1.507	.518
15	-1.052	.392	-1.174	.464	-1.238	.490	-1.304	.521	-1.626	.414	-1.472	.386
20	-.933	.304	-1.026	.378	-1.076	.399	-1.134	.428	-1.454	.328	-1.406	.315
25	-.835	.237	-.913	.301	-.965	.323	-1.006	.351	-1.248	.263	-1.299	.239
30	-.774	.186	-.837	.245	-.879	.268	-.918	.289	-1.051	.210	-1.188	.183
35	-.722	.144	-.786	.194	-.808	.217	-.846	.237	-.899	.141	-1.061	.122
40	-.649	.108	-.709	.153	-.732	.177	-.758	.201	-.753	.096	-.944	.081
45	-.577	.098	-.623	.143	-.641	.162	-.670	.175	-.586	.086	-.823	.056
50	-.503	.093	-.546	.133	-.565	.151	-.588	.165	-.546	.076	-.721	.041
55	-.438	.088	-.469	.122	-.485	.141	-.500	.155	-.470	.061	-.640	.030
60	-.366	.098	-.393	.128	-.404	.141	-.418	.155	-.359	.066	-.559	.030
65	-.289	.103	-.311	.128	-.323	.141	-.330	.155	-.359	.066	-.497	.025
70	-.222	.113	-.240	.138	-.242	.146	-.258	.155	-.308	.066	-.447	.025
75	-.155	.123	-.168	.143	-.172	.151	-.175	.160	-.263	.071	-.396	.005
80	-.088	.134	-.097	.153	-.106	.162	-.113	.170	-.222	.086	-.370	.010
85	-.041	.144	-.046	.163	-.045	.167	-.057	.175	-.187	.086	-.330	.005
90	.026	.160	.026	.178	.022	.187	.015	.186	-.146	.096	-.295	.005
95	.072	.165	.066	.178	.065	.182	.062	.186	-.121	.086	-.264	-.015

NACA

TABLE V.– PRESSURE DISTRIBUTION FOR THE NACA 64A006 AIRFOIL SECTION

Angle of Attack, α	PRESSURE COEFFICIENT, P													
	0°		1°		2°		3°		4°		4-1/2°		5°	
Chordwise Station (Percent chord)	Upper	Lower	Upper	Lower	Upper	Lower	Upper	Lower	Upper	Lower	Upper	Lower	Upper	Lower
0	1.000	---	0.834	---	0.247	---	0.743	---	-2.117	---	-2.985	---	-1.626	---
.033	.826	0.812	.242	0.990	-.798	0.914	-2.265	0.503	-4.120	-0.223	-5.260	-0.704	-2.675	-0.168
.100	.393	.510	-.349	.884	-1.440	1.000	-2.837	.909	-4.485	.559	-5.419	.323	-2.219	.536
.200	.163	.168	-.493	.626	-1.400	.909	-2.469	1.000	-3.762	.940	-4.910	.857	-2.300	.916
.333	.194	.102	-.545	.553	-1.293	.960	-2.230	1.000	-3.440	.985	-3.650	.944	-2.300	.974
.500	-.015	.010	-.540	.419	-1.202	.738	-2.101	.929	-2.680	.995	-3.190	1.000	-2.171	1.000
.667	-.061	-.015	-.515	.359	-1.086	.652	-1.710	.658	-2.355	.970	-2.775	1.000	-2.181	.994
.833	-.097	-.020	-.510	.308	-1.025	.581	-1.460	.768	-2.151	.929	-2.524	.974	-2.181	.959
1	-.101	-.015	-.480	.293	-.955	.556	-1.408	.761	-1.980	.984	-2.310	.954	-2.177	.934
1.50	-.117	-.056	-.434	.212	-.828	.445	-1.209	.633	-1.645	.782	-1.903	.852	-2.188	.836
2	-.128	-.092	-.394	.146	-.702	.367	-1.031	.546	-1.400	.695	-1.603	.776	-2.212	.766
2.50	-.123	-.092	-.359	.131	-.596	.333	-.918	.505	-1.239	.650	-1.423	.719	-2.145	.714
3	-.123	-.092	-.343	.106	-.566	.293	-.852	.359	-1.136	.594	-1.306	.668	-2.100	.663
4	-.133	-.101	-.309	.069	-.510	.227	-.745	.386	-.990	.518	-1.122	.582	-1.861	.582
5	-.143	-.112	-.308	.045	-.485	.197	-.683	.337	-.898	.454	-1.025	.520	-1.595	.500
7.50	-.138	-.117	-.273	.011	-.435	.142	-.572	.261	-.736	.412	-.939	.418	-1.091	.423
10	-.148	-.148	-.262	-.035	-.384	.081	-.511	.189	-.650	.284	-.730	.337	-.826	.342
12.50	-.158	-.133	-.252	-.031	-.367	.078	-.475	.168	-.594	.254	-.668	.301	-.704	.301
15	-.148	-.138	-.227	-.046	-.336	.046	-.434	.138	-.542	.213	-.604	.255	-.638	.260
20	-.153	-.143	-.227	-.066	-.316	.011	-.393	.093	-.487	.157	-.541	.199	-.556	.199
25	-.168	-.143	-.232	-.076	-.306	-.005	-.373	.066	-.457	.122	-.500	.152	-.505	.158
30	-.158	-.153	-.212	-.091	-.286	-.031	-.344	.036	-.467	.086	-.454	.123	-.464	.122
35	-.173	-.168	-.212	-.111	-.273	-.056	-.334	.006	-.396	.056	-.434	.077	-.439	.077
40	-.179	-.168	-.222	-.116	-.273	-.066	-.327	-.015	-.381	.036	-.408	.056	-.413	.056
45	-.168	-.158	-.207	-.111	-.253	-.066	-.296	-.020	-.340	.025	-.373	.046	-.377	.041
50	-.153	-.149	-.187	-.106	-.222	-.066	-.260	-.026	-.305	.020	-.333	.036	-.337	.031
55	-.133	-.128	-.182	-.086	-.197	-.051	-.235	-.015	-.269	.025	-.291	.036	-.290	.031
60	-.097	-.092	-.131	-.076	-.167	-.041	-.199	-.010	-.228	.025	-.250	.036	-.260	.031
65	-.082	-.077	-.121	-.056	-.142	-.025	-.194	0	-.193	.030	-.209	.036	-.214	.031
70	-.056	-.061	-.086	-.031	-.111	-.011	-.138	.015	-.173	.036	-.184	.041	-.179	.036
75	-.041	-.041	-.056	-.020	-.076	.011	-.097	.026	-.122	.041	-.133	.056	-.138	.041
80	-.020	-.010	-.041	-.046	-.056	.025	-.077	.036	-.086	.046	-.097	.056	-.102	.046
85	0	0	-.061	.015	-.020	.035	-.041	.046	-.050	.061	-.061	.066	-.071	.046
90	.031	.031	.020	.031	-.011	.046	-.006	.055	-.015	.071	-.015	.077	-.036	.051
95	.056	.056	.051	.061	.051	.066	.041	.077	.041	.081	.036	.087	.015	.066

Angle of Attack, α	PRESSURE COEFFICIENT, P													
	5-1/2°		6°		7°		8°		9°		10°		11°	
Chordwise Station (Percent chord)	Upper	Lower	Upper	Lower	Upper	Lower	Upper	Lower	Upper	Lower	Upper	Lower	Upper	Lower
0	-1.279	---	-1.250	---	-1.143	---	-1.045	---	-0.966	---	-0.675	---	-0.940	---
.033	-2.040	-0.066	-1.840	-0.066	-1.496	-0.082	-1.080	-0.061	-1.184	-0.036	-1.045	0.055	-.873	-0.480
.100	-1.176	.572	-1.540	.566	-1.289	.520	-1.186	.528	-1.056	.536	-.903	.584	-.868	.470
.200	-1.721	.920	-1.550	.914	-1.294	.880	-1.131	.878	-1.061	.882	-.908	.888	-.868	.842
.333	-1.731	.975	-1.555	.959	-1.299	.940	-1.131	.938	-1.061	.949	-.908	.944	-.868	.965
.500	-1.731	1.000	-1.555	1.000	-1.299	.996	-1.131	1.000	-1.061	1.000	-.903	.995	-.868	1.000
.667	-1.726	.996	-1.550	1.000	-1.294	.996	-1.131	1.000	-1.056	1.000	-.908	.995	-.863	1.000
.833	-1.721	.960	-1.545	.974	-1.294	.976	-1.131	.990	-1.056	.995	-.903	.970	-.858	.995
1	-1.716	.944	-1.540	.954	-1.284	.960	-1.131	.974	-1.051	.985	-.903	.960	-.858	.975
1.50	-1.716	.852	-1.535	.868	-1.284	.884	-1.127	.898	-1.046	.908	-.898	.888	-.852	.914
2	-1.726	.827	-1.545	.810	-1.344	.920	-1.126	.842	-1.036	.852	-.898	.828	-.848	.852
2.50	-1.731	.730	-1.550	.755	-1.294	.778	-1.127	.802	-1.036	.812	-.898	.782	-.848	.806
3	-1.735	.679	-1.555	.730	-1.299	.732	-1.127	.756	-1.036	.766	-.898	.751	-.848	.761
4	-1.741	.602	-1.565	.625	-1.309	.652	-1.133	.680	-1.040	.694	-.898	.670	-.848	.700
5	-1.745	.536	-1.592	.562	-1.319	.596	-1.147	.619	-1.051	.631	-.914	.610	-.858	.620
7.50	-1.617	.444	-1.586	.464	-1.349	.500	-1.173	.521	-1.076	.532	-.989	.513	-.863	.531
10	-1.368	.362	-1.520	.385	-1.360	.415	-1.194	.442	-1.087	.444	-.939	.422	-.873	.460
12.50	-1.107	.322	-1.397	.347	-1.364	.379	-1.203	.396	-1.103	.398	-.950	.376	-.884	.444
15	-.882	.281	-1.245	.301	-1.330	.334	-1.208	.350	-1.112	.347	-.954	.333	-.894	.135
20	-.628	.214	-.918	.240	-1.243	.268	-1.198	.279	-1.118	.276	-.974	.254	-.909	.276
25	-.526	.174	-.674	.194	-1.101	.217	-1.153	.228	-1.107	.219	-.980	.198	-.918	.204
30	-.459	.138	-.532	.148	-.935	.172	-1.081	.188	-1.072	.168	-.975	.142	-1.036	.158
35	-.429	.097	-.454	.101	-.768	.096	-.995	.122	-1.025	.112	-.954	.094	-.929	.102
40	-.403	.072	-.417	.077	-.631	.081	-.894	.091	-.980	.077	-.939	.056	-.914	.051
45	-.367	.056	-.373	.061	-.520	.056	-.787	.071	-.904	.051	-.909	.015	-.904	.020
50	-.327	.046	-.332	.055	-.424	.051	-.680	.051	-.838	.031	-.868	0	-.883	0
55	-.296	.046	-.301	.046	-.369	.045	-.592	.046	-.765	.020	-.828	-.015	-.854	-.026
60	-.255	.046	-.265	.046	-.308	.040	-.503	.036	-.684	.010	-.787	-.025	-.832	-.046
65	-.198	.046	-.240	.046	-.268	.035	-.442	.025	-.631	-.005	-.746	-.046	-.800	-.051
70	-.189	.046	-.199	.046	-.227	.040	-.365	.015	-.556	-.005	-.701	-.061	-.766	-.081
75	-.143	.046	-.158	.046	-.212	.040	-.307	.015	-.500	-.026	-.665	-.081	-.735	-.097
80	-.112	.051	-.128	.041	-.161	.035	-.274	.010	-.454	-.046	-.624	-.102	-.710	-.123
85	-.082	.051	-.092	.041	-.126	.025	-.234	-.005	-.398	-.061	-.588	-.127	-.674	-.158
90	-.035	.051	-.056	.041	-.110	.015	-.193	-.021	-.362	-.092	-.538	-.167	-.628	-.199
95	.005	.051	-.020	.041	-.071	.011	-.163	-.046	-.316	-.128	-.482	-.218	-.572	-.271

NACA

TABLE VI.– PRESSURE DISTRIBUTION FOR THE DOUBLE-WEDGE AIRFOIL SECTION

	PRESSURE COEFFICIENT, P																	
Angle of Attack, α	0°		1°		2°		3°		4°		5°		6°		7°		8°	
Chordwise Station (Percent chord)	Upper	Lower	Upper	Lower	Upper	Lower	Upper	Lower	Upper	Lower	Upper	Lower	Upper	Lower	Upper	Lower	Upper	Lower
0	1.000	- - -	0.810	- - -	0.300	- - -	-0.320	- - -	-1.025	- - -	-1.000	- - -	-1.000	- - -	-0.930	- - -	-0.860	- - -
1.25	.150	- - -	-.060	- - -	-.920	- - -	-1.030	- - -	-.980	- - -	-.980	- - -	-1.000	- - -	-.930	- - -	-.860	- - -
2.50	.090	0.090	-.080	0.330	-1.000	0.410	-1.060	0.490	-1.000	0.600	-1.000	0.680	-1.005	0.720	-.930	0.790	-.865	0.780
5	.065	.065	-.070	.200	-.390	.315	-1.055	.375	-1.015	.460	-1.015	.550	-1.020	.585	-.940	.610	-.875	.600
7.50	.055	.055	-.060	.145	-.170	.260	-.940	.325	-1.030	.390	-1.030	.475	-1.030	.500	-.950	.545	-.890	.540
10	.050	.050	-.060	.115	-.140	.225	-.700	.280	-1.010	.345	-1.040	.420	-1.050	.440	-.965	.490	-.900	.475
12.50	.040	.040	-.060	.100	-.145	.200	-.400	.255	-.945	.320	-1.035	.375	-1.055	.395	-.975	.450	-.910	.445
15	.025	.025	-.060	.080	-.150	.180	-.270	.225	-.825	.285	-1.035	.340	-1.065	.360	-.995	.400	-.920	.410
20	.005	.005	-.060	.050	-.155	.140	-.190	.175	-.550	.235	-.980	.285	-1.080	.295	-1.015	.345	-.940	.335
25	-.010	-.010	-.070	.035	-.150	.115	-.190	.140	-.330	.195	-.845	.240	-1.050	.240	-1.025	.300	-.950	.285
30	-.020	-.020	-.085	.015	-.145	.080	-.200	.100	-.230	.160	-.670	.200	-.970	.200	-1.010	.260	-.955	.235
35	-.040	-.040	-.110	-.015	-.165	.055	-.225	.055	-.210	.120	-.500	.160	-.870	.155	-.970	.210	-.950	.190
40	-.080	-.080	-.145	-.050	-.200	.020	-.250	.010	-.225	.080	-.365	.120	-.740	.110	-.905	.160	-.920	.130
45	-.120	-.120	-.200	-.095	-.240	-.040	-.270	-.045	-.240	.030	-.290	.175	-.600	.050	-.820	.090	-.870	.070
50	-.150	-.150	-.210	-.125	-.235	-.070	-.280	-.070	-.250	-.015	-.250	.015	-.460	.005	-.725	.040	-.810	.020
55	-.130	-.130	-.180	-.115	-.210	-.075	-.255	-.075	-.235	-.025	-.215	.005	-.370	-.005	-.620	.025	-.740	-.010
60	-.095	-.095	-.140	-.080	-.160	-.035	-.200	-.060	-.190	.010	-.190	.030	-.300	.020	-.515	.045	-.675	.010
65	-.055	-.055	-.090	-.040	-.110	0	-.160	-.040	-.145	.040	-.160	.055	-.250	.040	-.430	.065	-.610	.030
70	-.025	-.025	-.055	-.010	-.070	.030	-.125	-.015	-.110	.050	-.135	.080	-.200	.050	-.355	.080	-.540	.035
75	-.010	-.010	-.030	.010	-.050	.025	-.080	0	-.080	.060	-.100	.085	-.160	.055	-.310	.080	-.470	.035
80	.010	.010	0	.020	-.040	.025	-.055	.020	-.060	.060	-.070	.085	-.140	.045	-.260	.065	-.410	.020
85	.035	.035	.020	.030	-.015	.030	-.040	.020	-.040	.060	-.050	.075	-.115	.030	-.220	.045	-.365	-.010
90	.050	.050	.035	.040	.010	.045	-.030	.020	-.010	.060	-.030	.065	-.095	.010	-.170	.015	-.320	-.045
95	.070	.070	.045	.050	.050	.065	.010	.030	.030	.060	.015	.050	-.060	0	-.140	-.020	-.290	-.090

	PRESSURE COEFFICIENT, P															
Angle of Attack, α	9°		10°		11°		12°		13°		14°		15°		16°	
Chordwise Station (Percent chord)	Upper	Lower	Upper	Lower	Upper	Lower	Upper	Lower	Upper	Lower	Upper	Lower	Upper	Lower	Upper	Lower
0	-0.820	- - -	-0.765	- - -	-0.730	- - -	-0.680	- - -	-0.700	- - -	-0.700	- - -	-0.780	- - -	-0.820	- - -
1.25	-.820	- - -	-.765	- - -	-.730	- - -	-.690	- - -	-.700	- - -	-.700	- - -	-.780	- - -	-.820	- - -
2.50	-.820	0.800	-.765	0.800	-.735	0.820	-.695	0.820	-.705	0.840	-.700	0.880	-.780	0.900	-.820	0.920
5	-.825	.670	-.770	.670	-.740	.670	-.700	.640	-.710	.680	-.705	.690	-.790	.700	-.825	.750
7.50	-.830	.560	-.775	.565	-.745	.565	-.700	.540	-.715	.580	-.705	.600	-.790	.620	-.830	.650
10	-.840	.500	-.785	.510	-.750	.510	-.710	.470	-.715	.510	-.710	.520	-.795	.550	-.830	.580
12.50	-.850	.450	-.800	.455	-.760	.455	-.720	.425	-.725	.465	-.715	.470	-.800	.490	-.840	.520
15	-.860	.400	-.810	.410	-.770	.410	-.725	.380	-.730	.420	-.720	.420	-.810	.440	-.840	.470
20	-.875	.330	-.820	.340	-.780	.340	-.730	.300	-.745	.340	-.735	.335	-.810	.360	-.840	.395
25	-.890	.270	-.830	.280	-.790	.280	-.750	.230	-.765	.270	-.755	.270	-.815	.290	-.840	.320
30	-.900	.215	-.835	.230	-.810	.230	-.770	.180	-.780	.200	-.770	.210	-.820	.230	-.850	.255
35	-.900	.175	-.840	.170	-.820	.170	-.780	.120	-.800	.130	-.780	.140	-.820	.160	-.860	.180
40	-.890	.130	-.840	.110	-.825	.110	-.790	.060	-.805	.060	-.790	.070	-.830	.090	-.880	.090
45	-.880	.060	-.825	.040	-.830	.040	-.795	-.020	-.810	-.020	-.800	-.020	-.850	0	-.890	.010
50	-.870	0	-.800	-.020	-.830	-.020	-.795	-.090	-.820	-.110	-.810	-.080	-.860	-.080	-.910	-.060
55	-.810	-.020	-.775	-.050	-.820	-.050	-.800	-.130	-.830	-.140	-.810	-.130	-.875	-.130	-.915	-.110
60	-.750	0	-.765	-.060	-.810	-.060	-.800	-.125	-.830	-.130	-.810	-.130	-.885	-.130	-.925	-.130
65	-.715	0	-.750	-.050	-.800	-.050	-.800	-.130	-.830	-.130	-.820	-.140	-.890	-.140	-.930	-.140
70	-.670	-.005	-.735	-.055	-.790	-.070	-.800	-.140	-.830	-.140	-.830	-.160	-.890	-.170	-.935	-.165
75	-.630	-.015	-.710	-.060	-.775	-.080	-.800	-.170	-.830	-.170	-.835	-.200	-.900	-.210	-.950	-.190
80	-.595	-.040	-.675	-.090	-.750	-.120	-.795	-.220	-.830	-.220	-.840	-.250	-.900	-.260	-.970	-.250
85	-.540	-.075	-.640	-.140	-.730	-.175	-.790	-.290	-.815	-.290	-.835	-.310	-.895	-.320	-.955	-.335
90	-.490	-.125	-.600	-.200	-.700	-.240	-.760	-.345	-.800	-.370	-.820	-.375	-.885	-.400	-.940	-.435
95	-.430	-.175	-.550	-.270	-.660	-.320	-.710	-.420	-.750	-.450	-.790	-.475	-.860	-.510	-.910	-.540

NACA

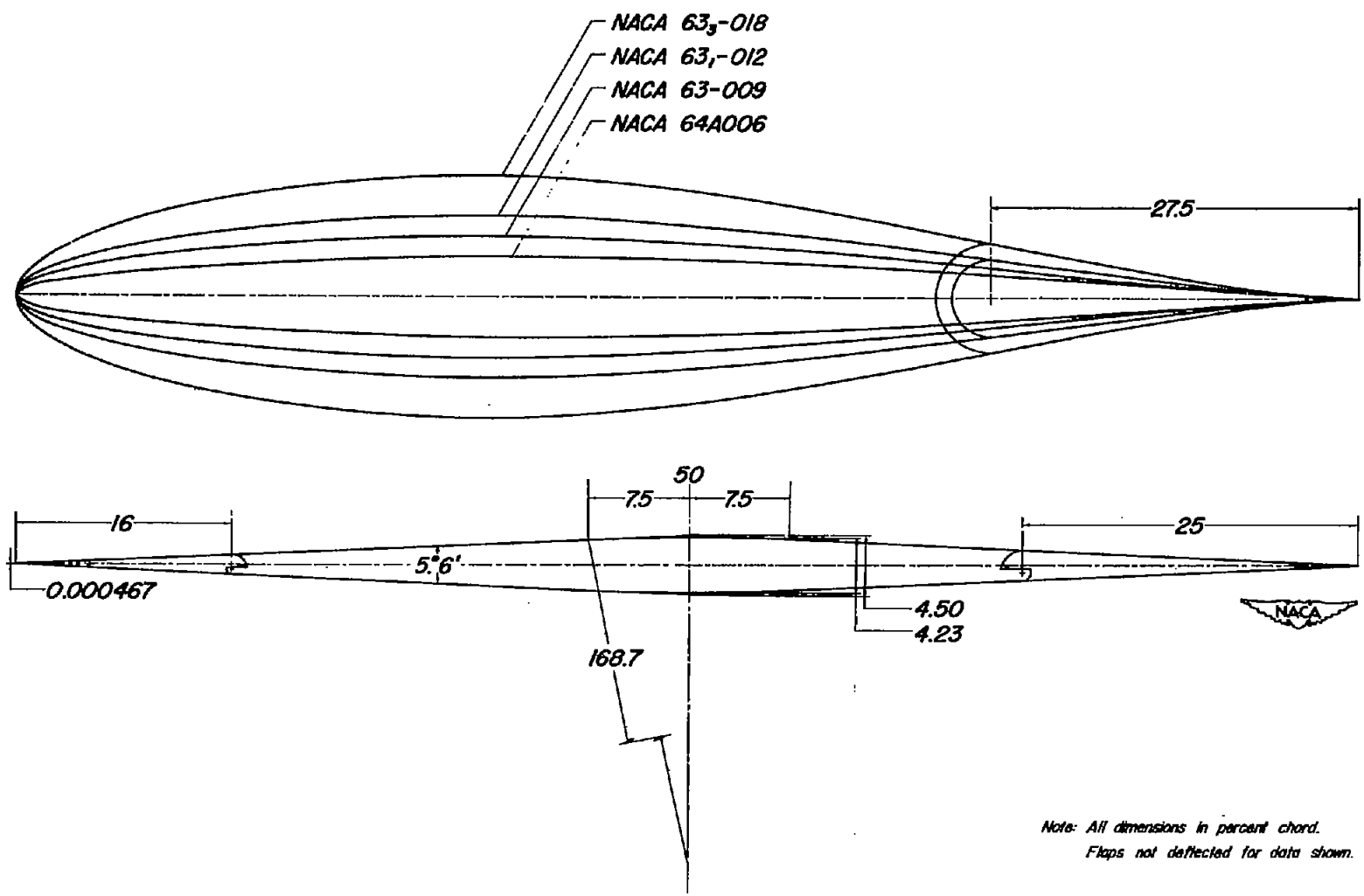

Figure 1.– Profiles of the five airfoil sections.

Figure 2.- Typical model installation.

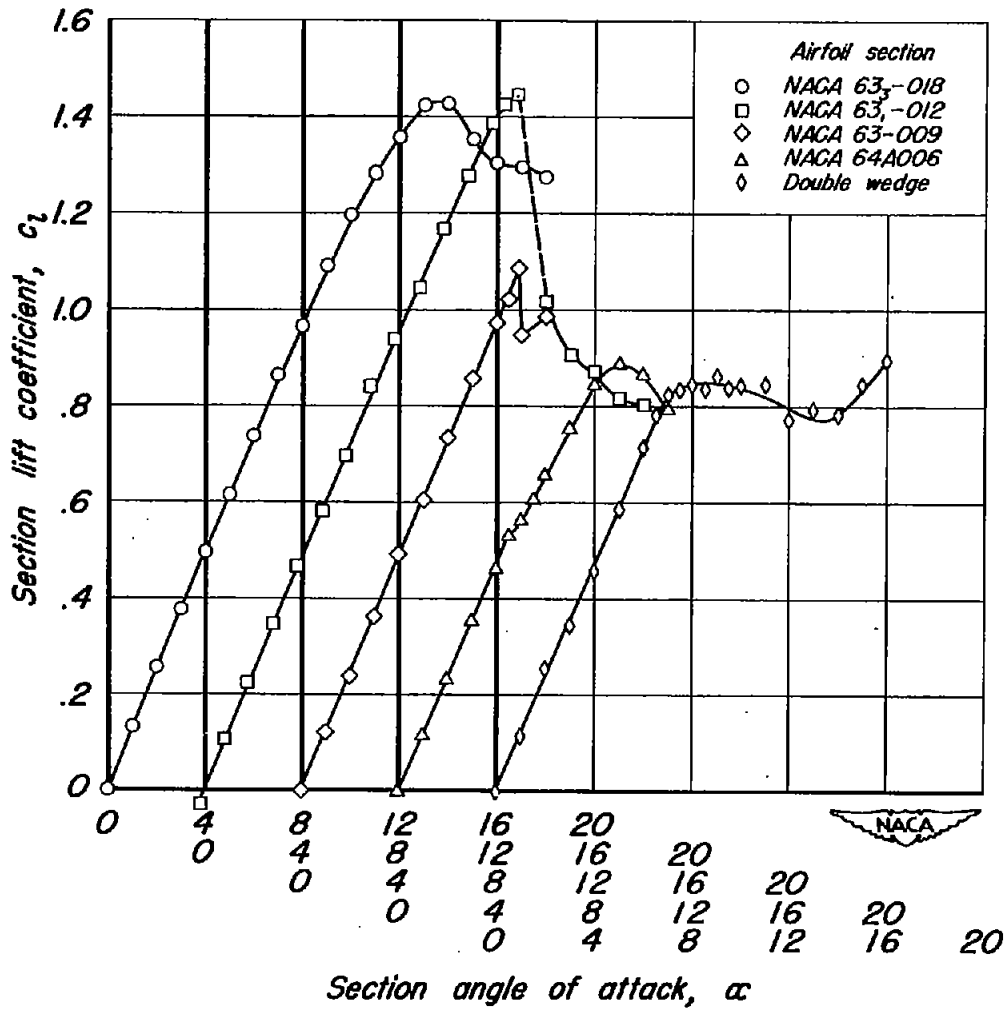

(a) Lift.

Figure 3.– Aerodynamic characteristics of the five airfoil sections. Reynolds number, 5,800,000.

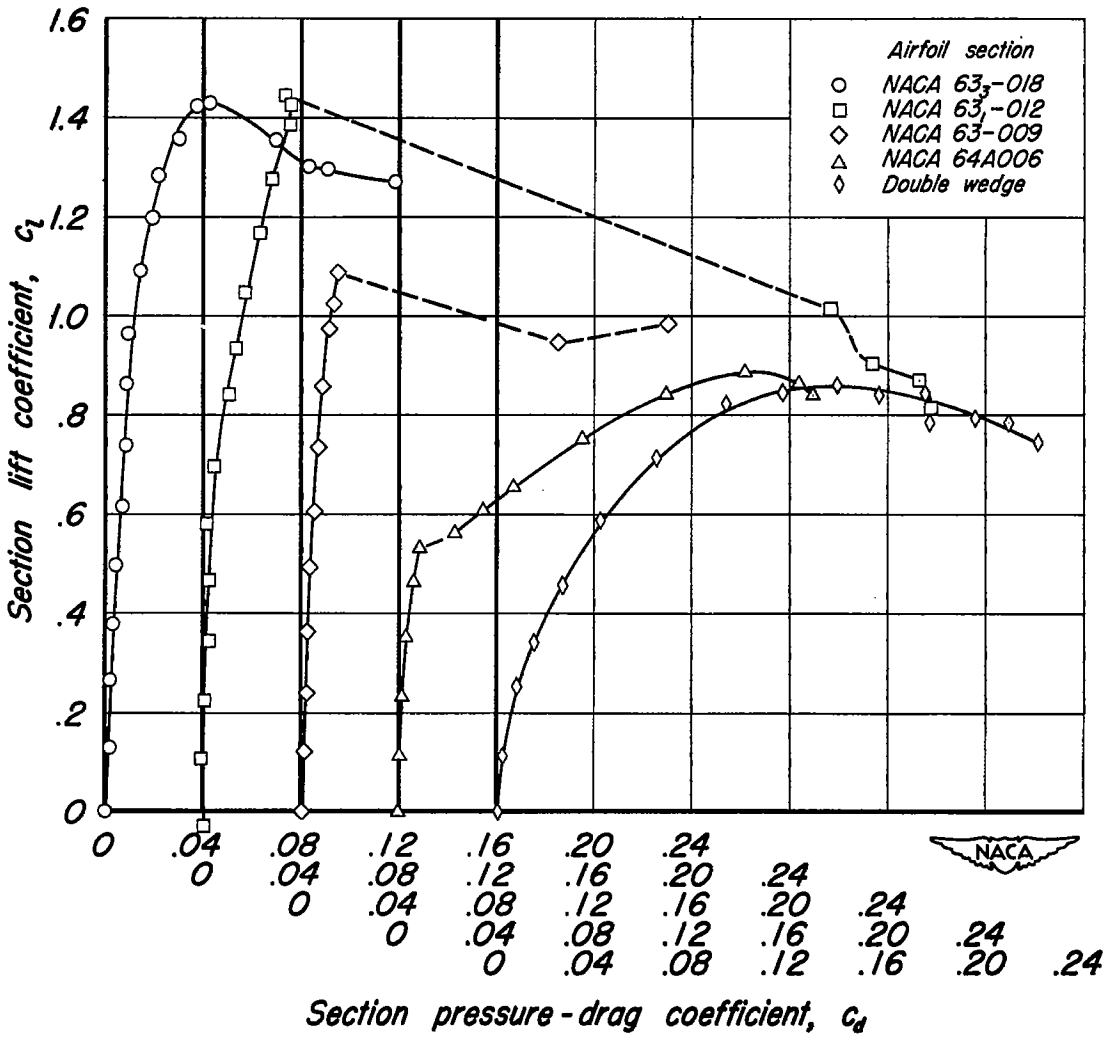

(b) Pressure drag.

Figure 3.– Continued.

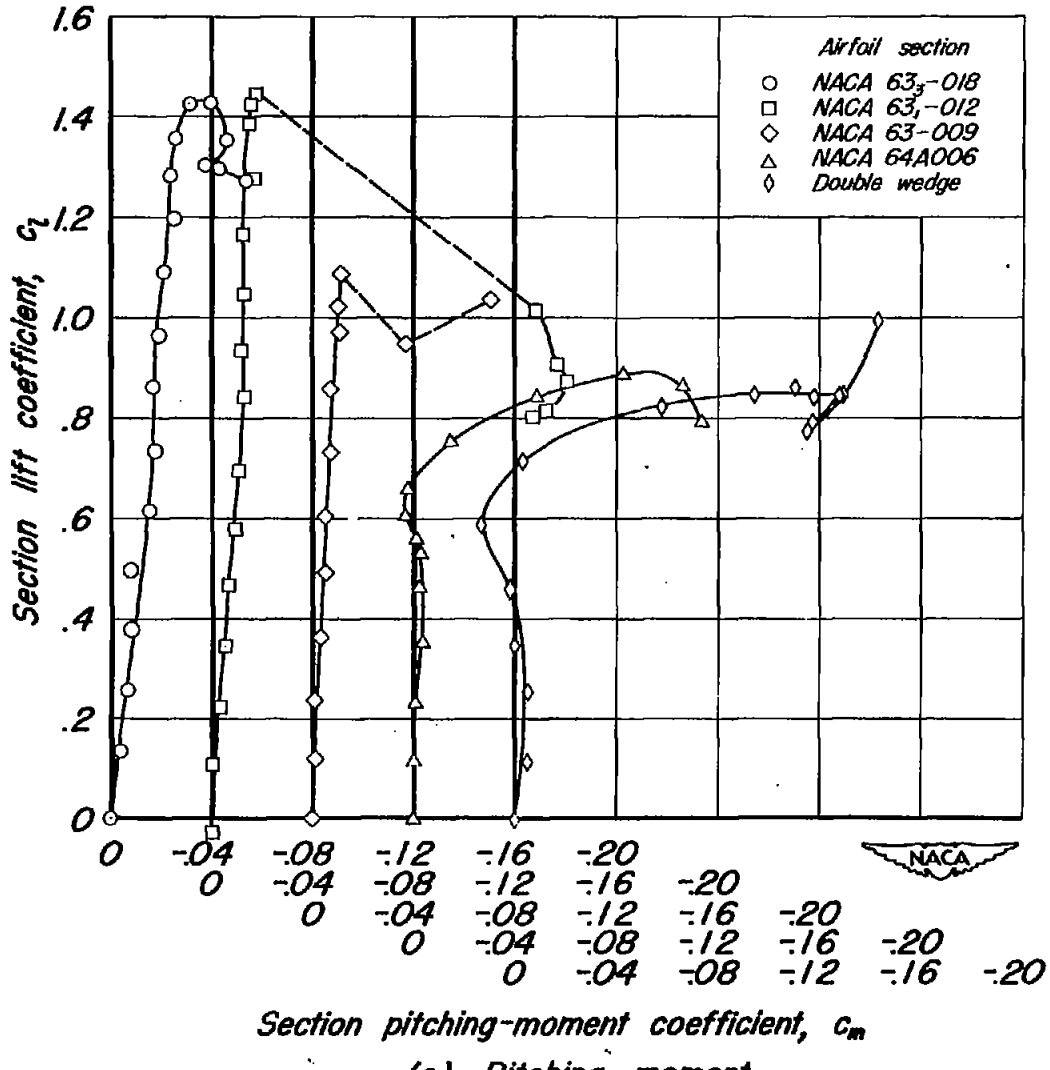

(c) Pitching moment.

Figure 3.– Concluded.

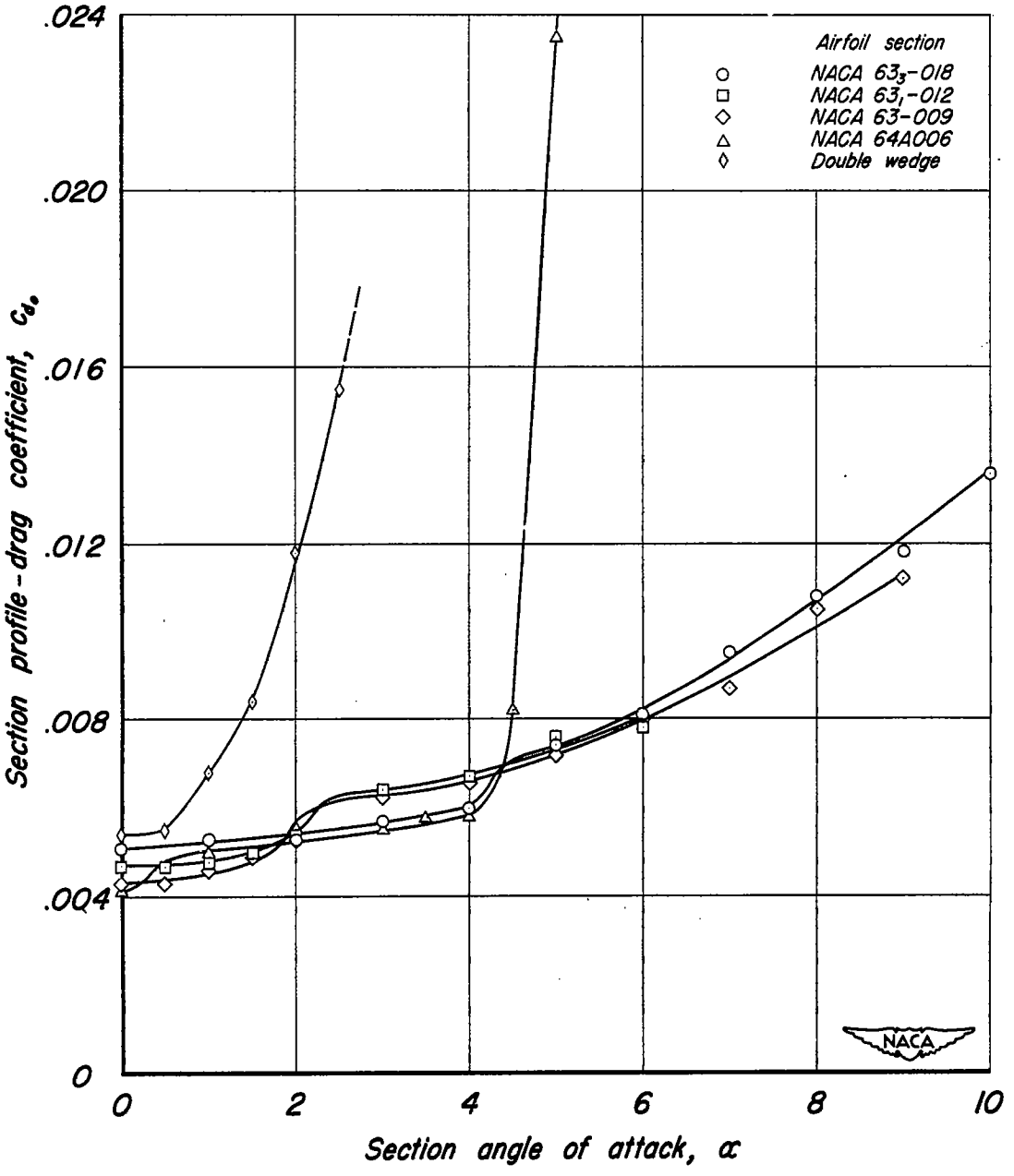

Figure 4.– Profile-drag characteristics of the five airfoil sections.

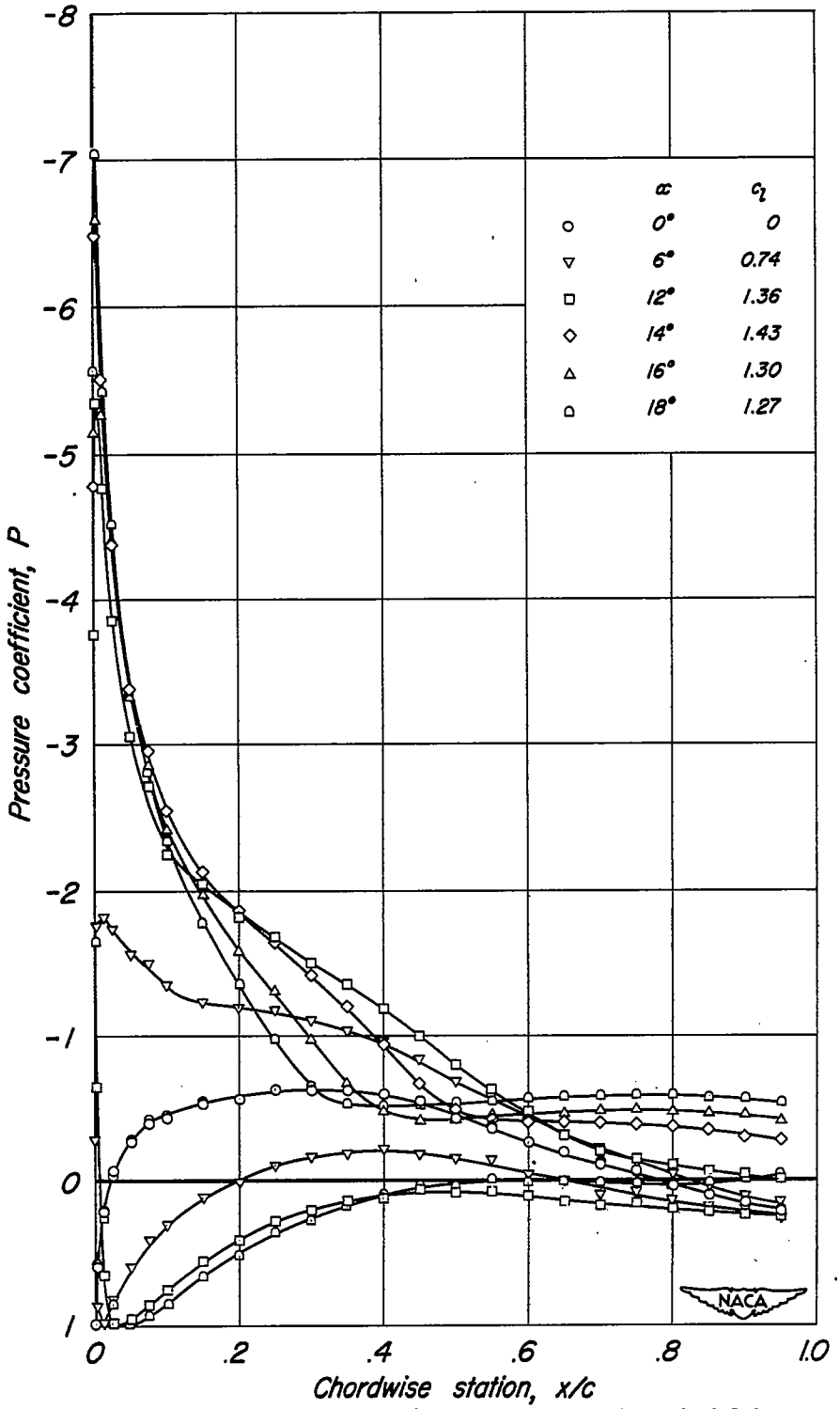

Figure 5.– Pressure distribution over the NACA 63_3-018 airfoil section.

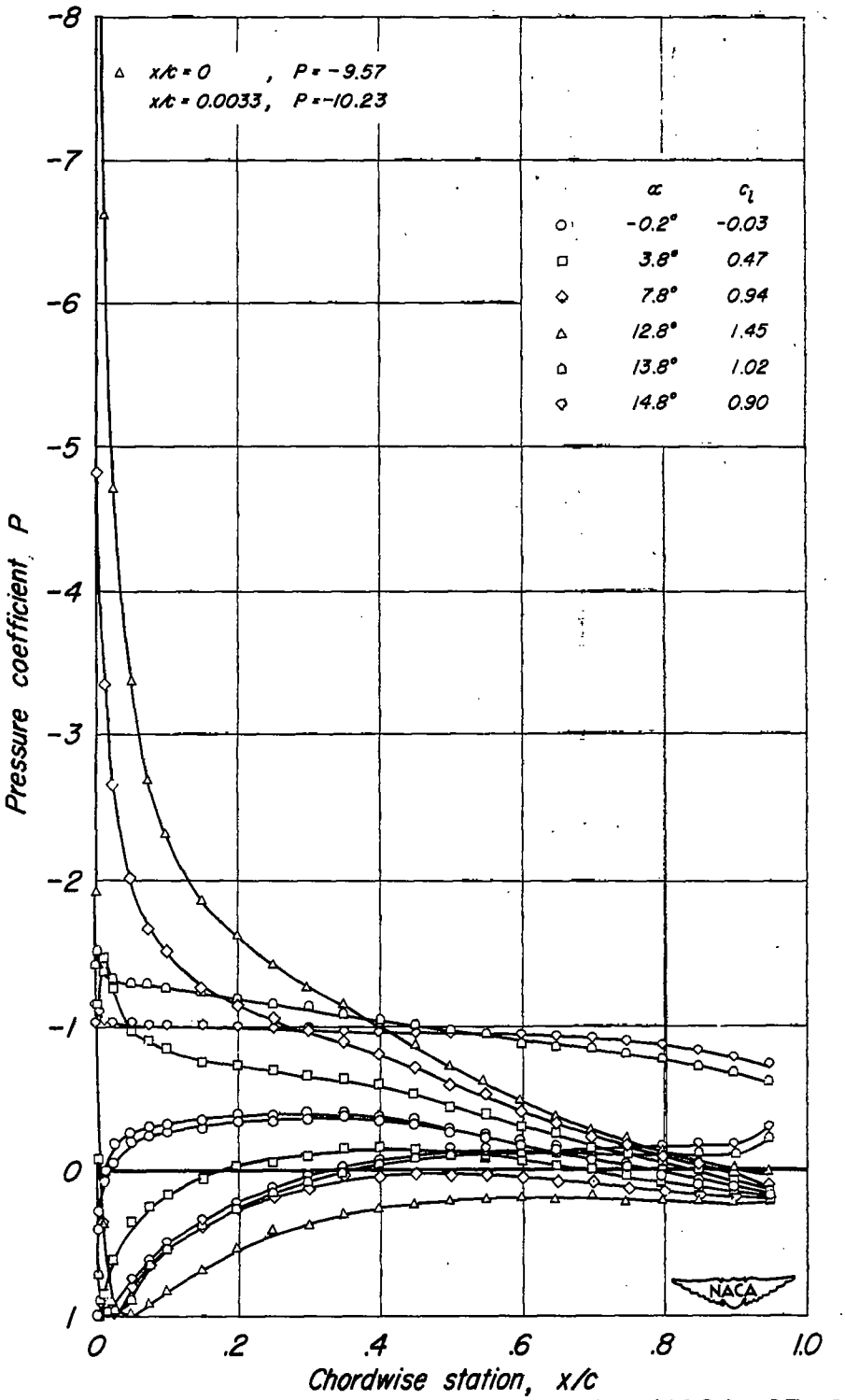

Figure 6.- Pressure distribution over the NACA 63,-012 airfoil section.

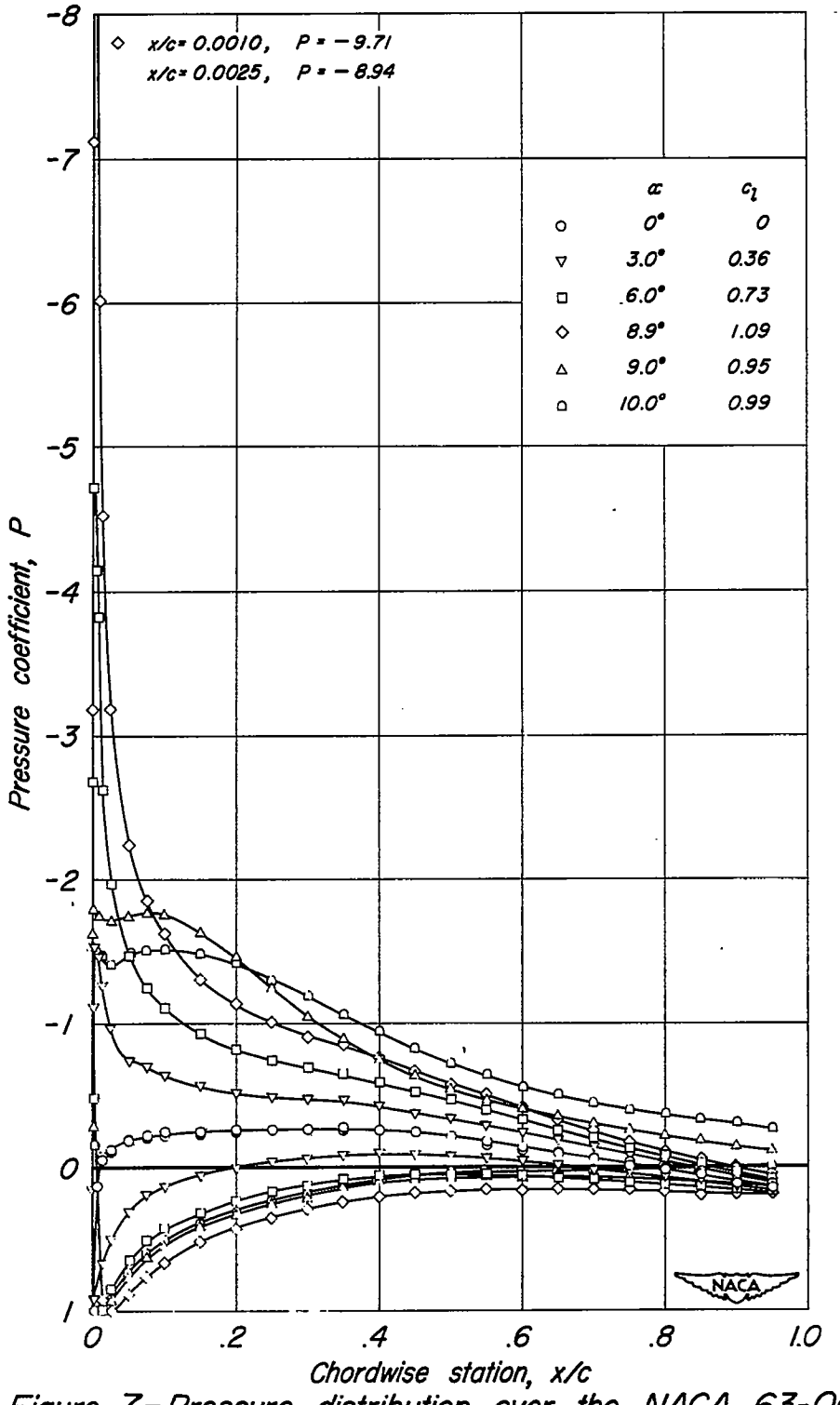

Figure 7.-Pressure distribution over the NACA 63-009 airfoil section.

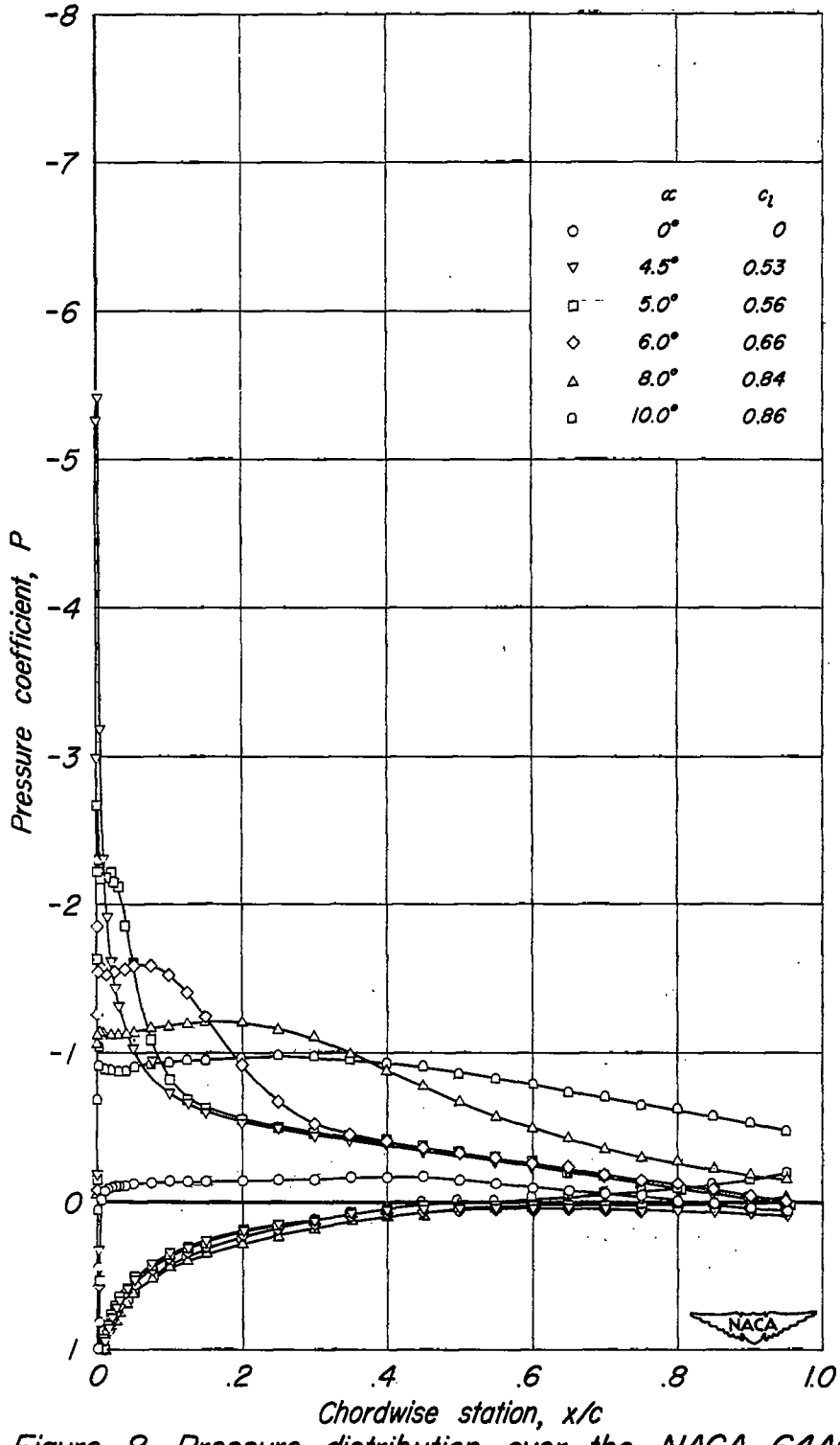

Figure 8.- Pressure distribution over the NACA 64A006 airfoil section.

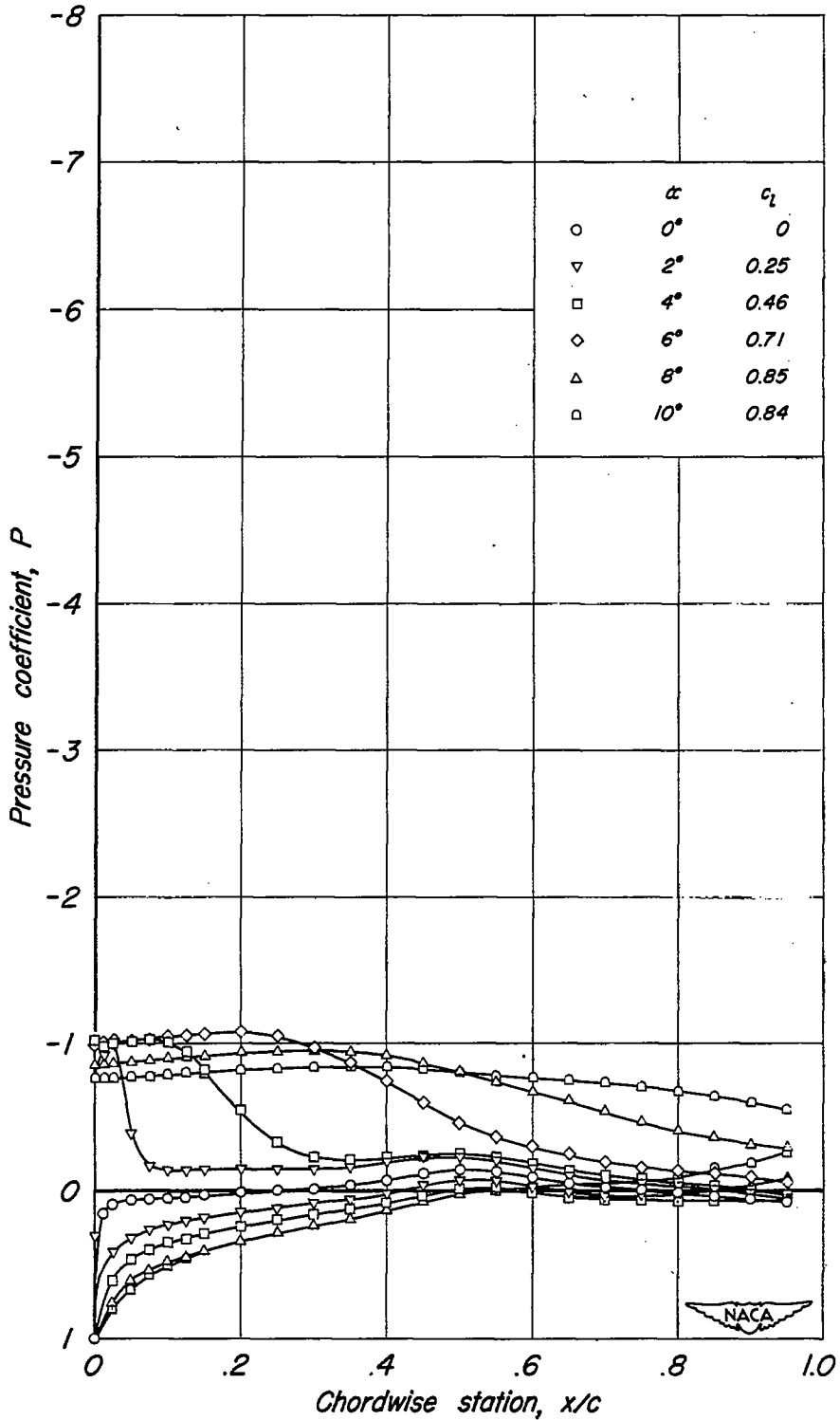

Figure 9.- Pressure distribution over the 4.23-percent-thick double-wedge airfoil section.

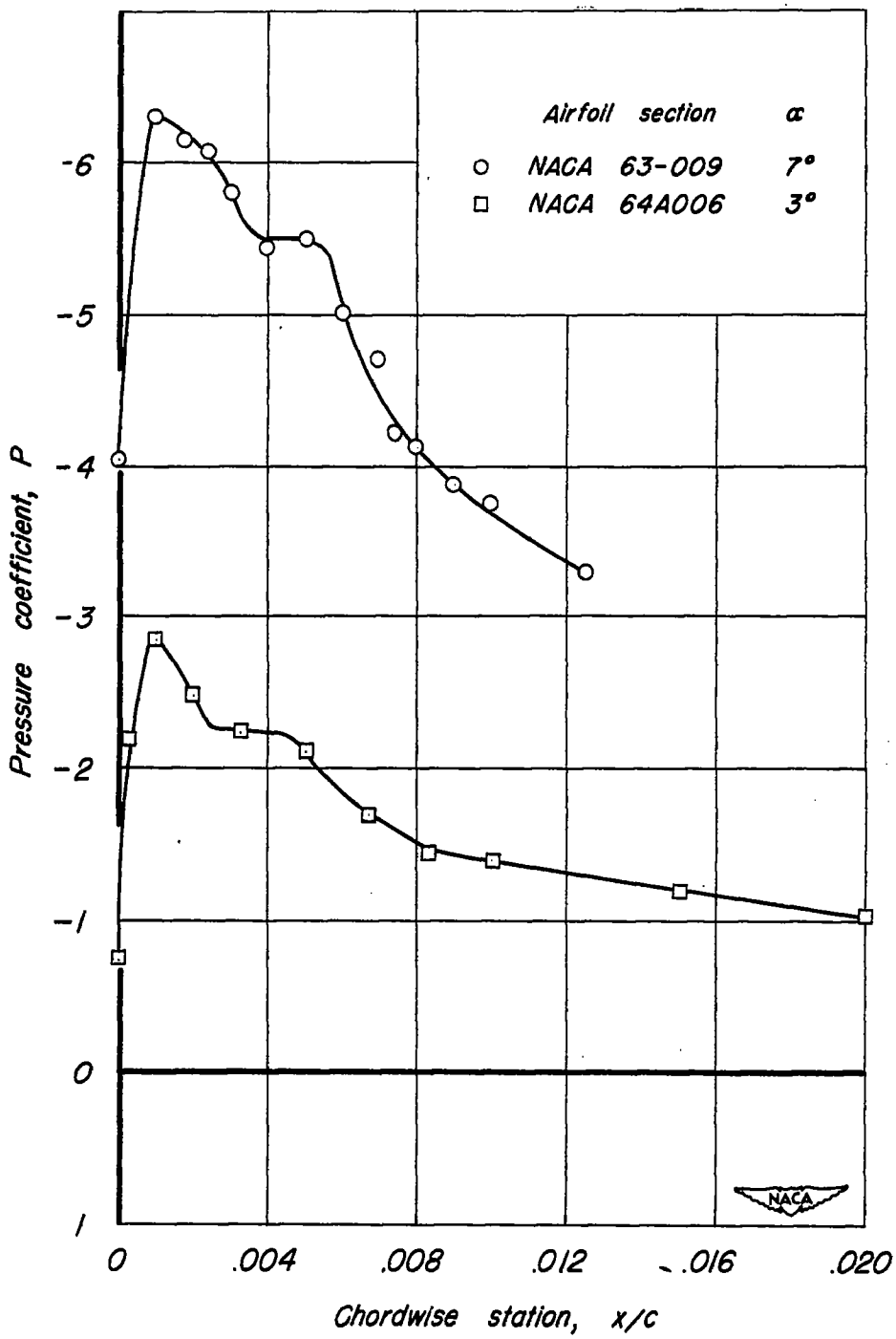

Figure 10.–Detailed pressure distribution in the vicinity of the bubble of laminar separation

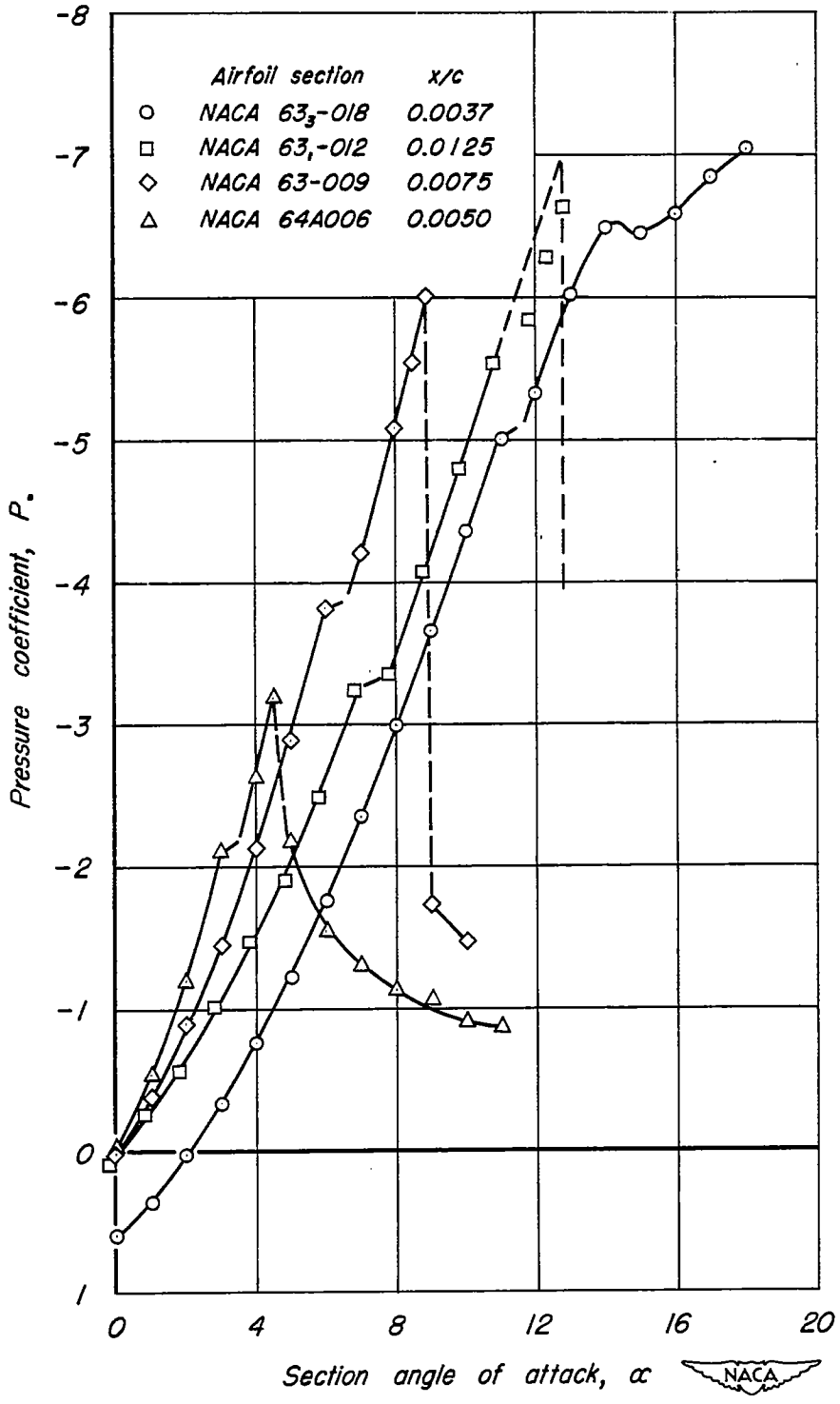

Figure 11.– The variation of pressure coefficient at particular chordwise stations with angle of attack.

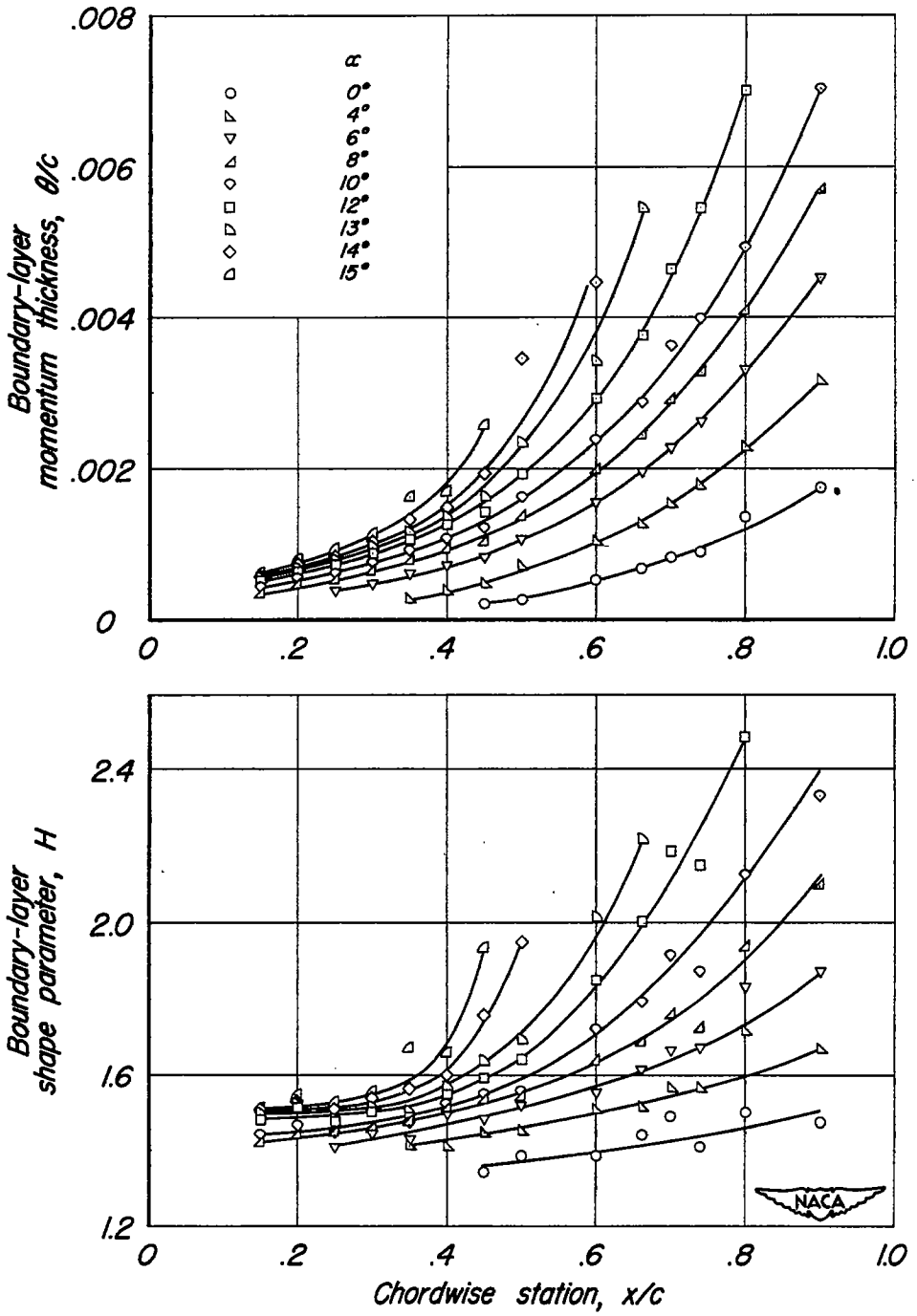

Figure 12.- Boundary-layer parameters for the NACA 63_3-018 airfoil section.

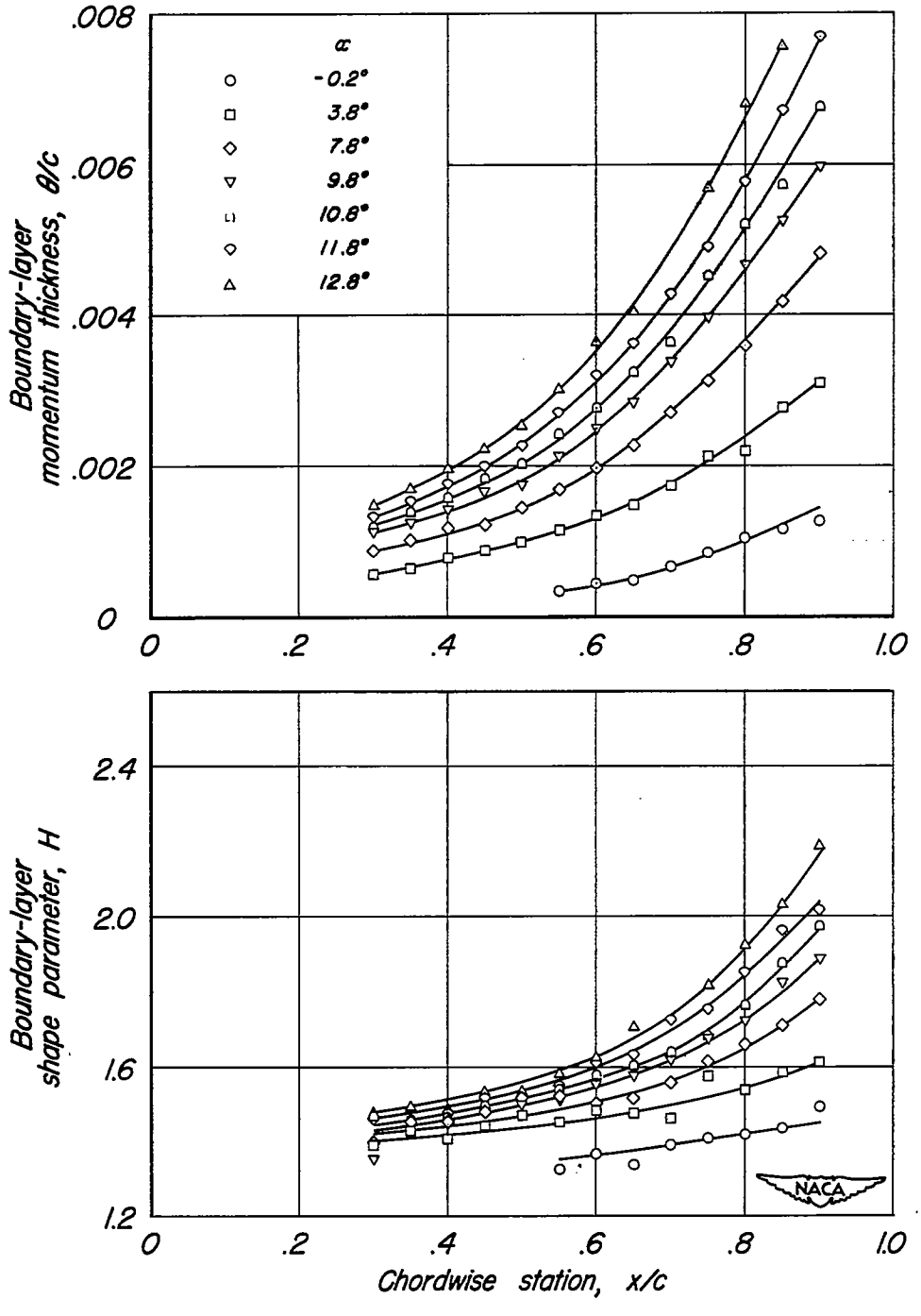

Figure 13.- Boundary-layer parameters for the NACA 63,-012 airfoil section.

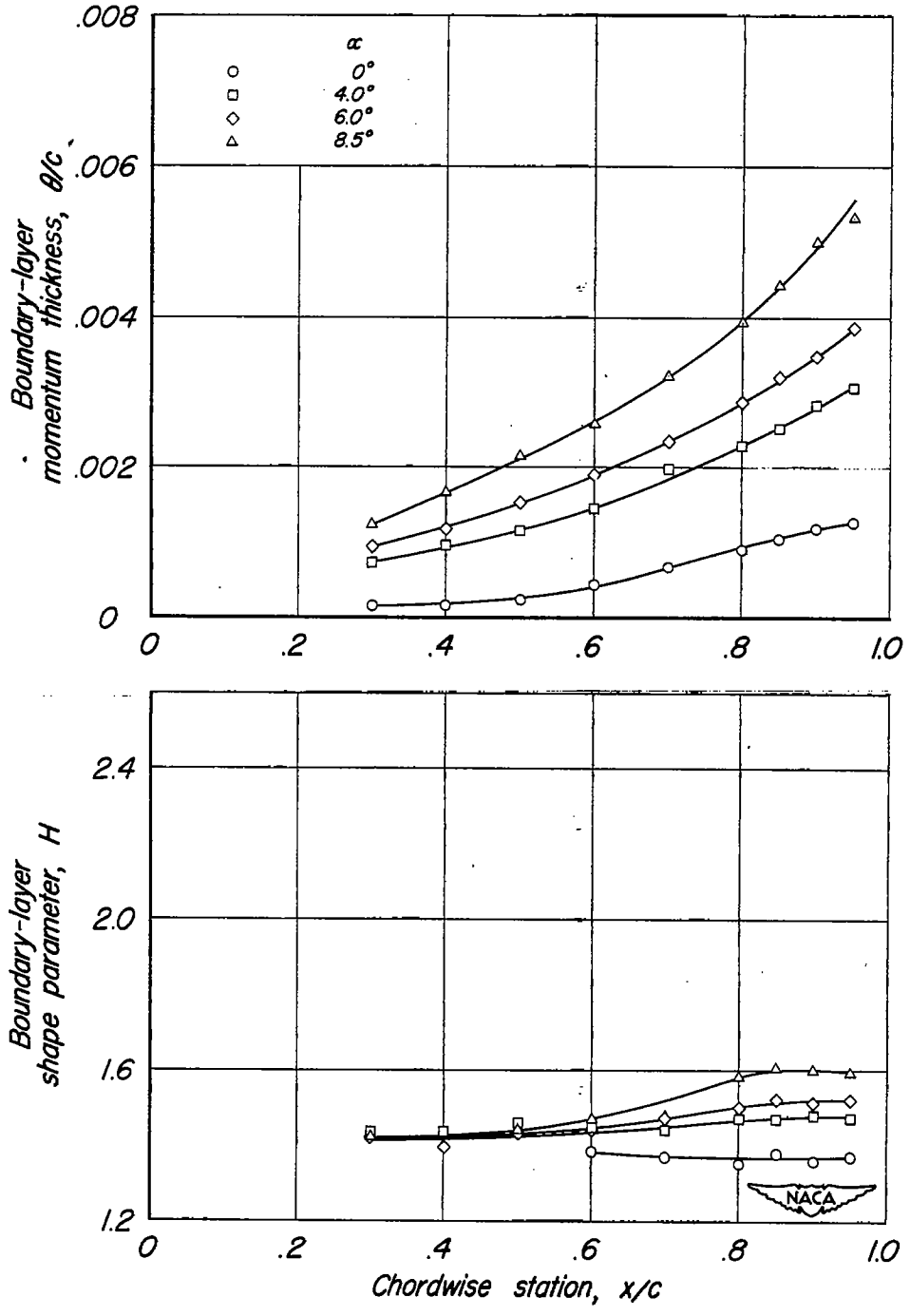

Figure 14.-Boundary-layer parameters for the NACA 63-009 airfoil section.

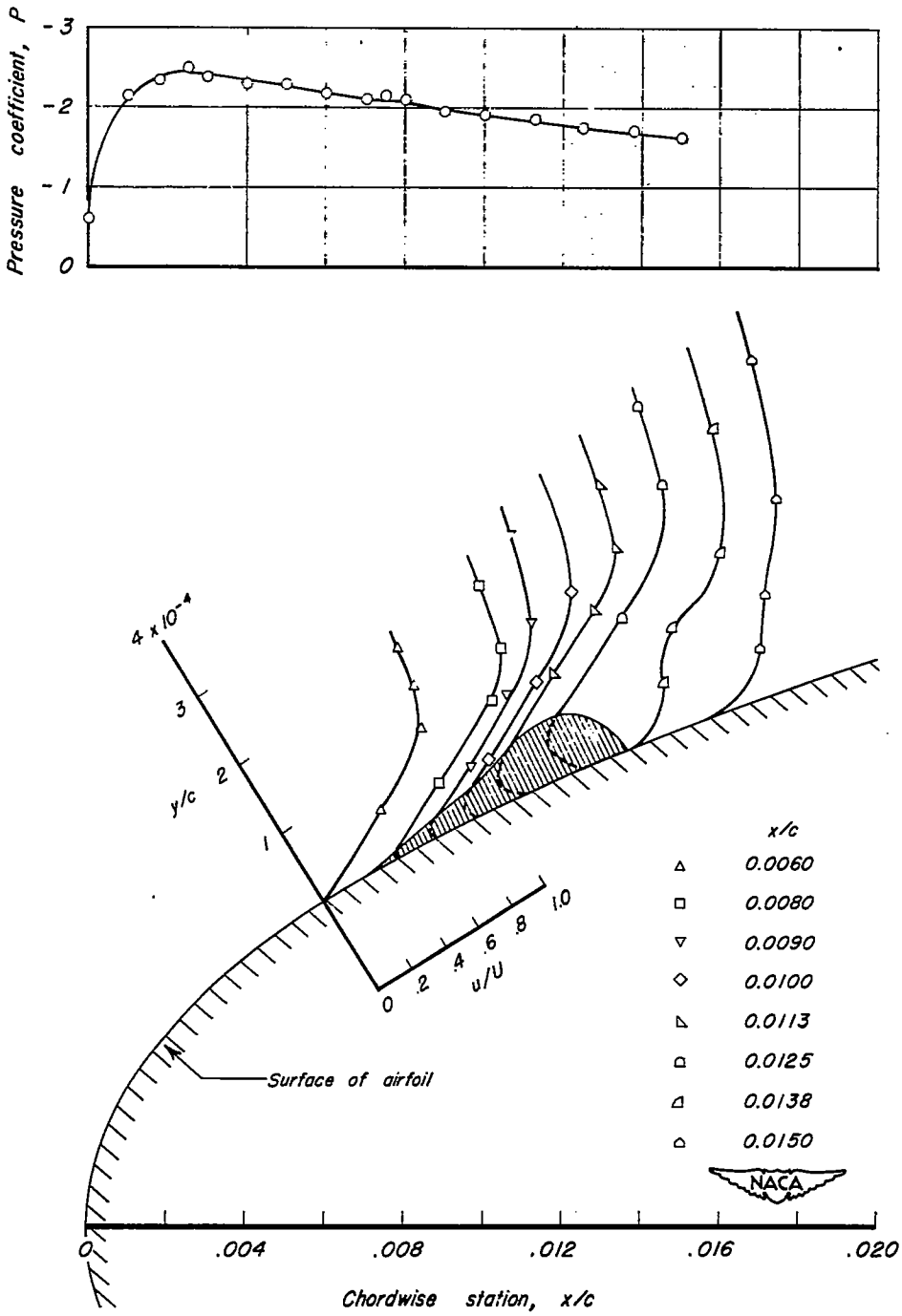

(a) $\alpha = 4°$.

Figure 15.- Pressure distributions and boundary-layer velocity profiles in the bubble of separated flow near the leading edge of the NACA 63-009 airfoil section.

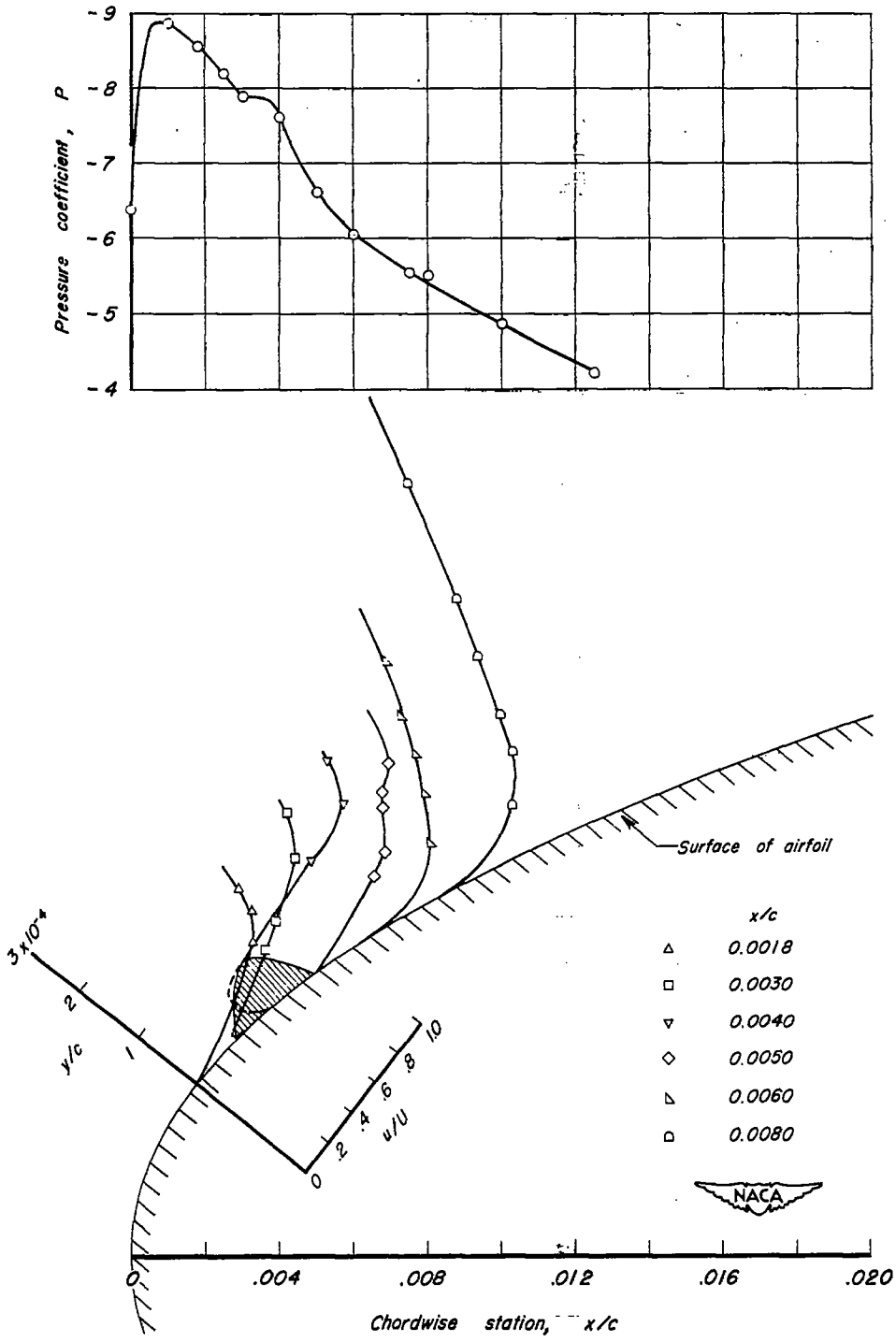

(b) $\alpha = 8.5°$.

Figure 15.- Concluded.

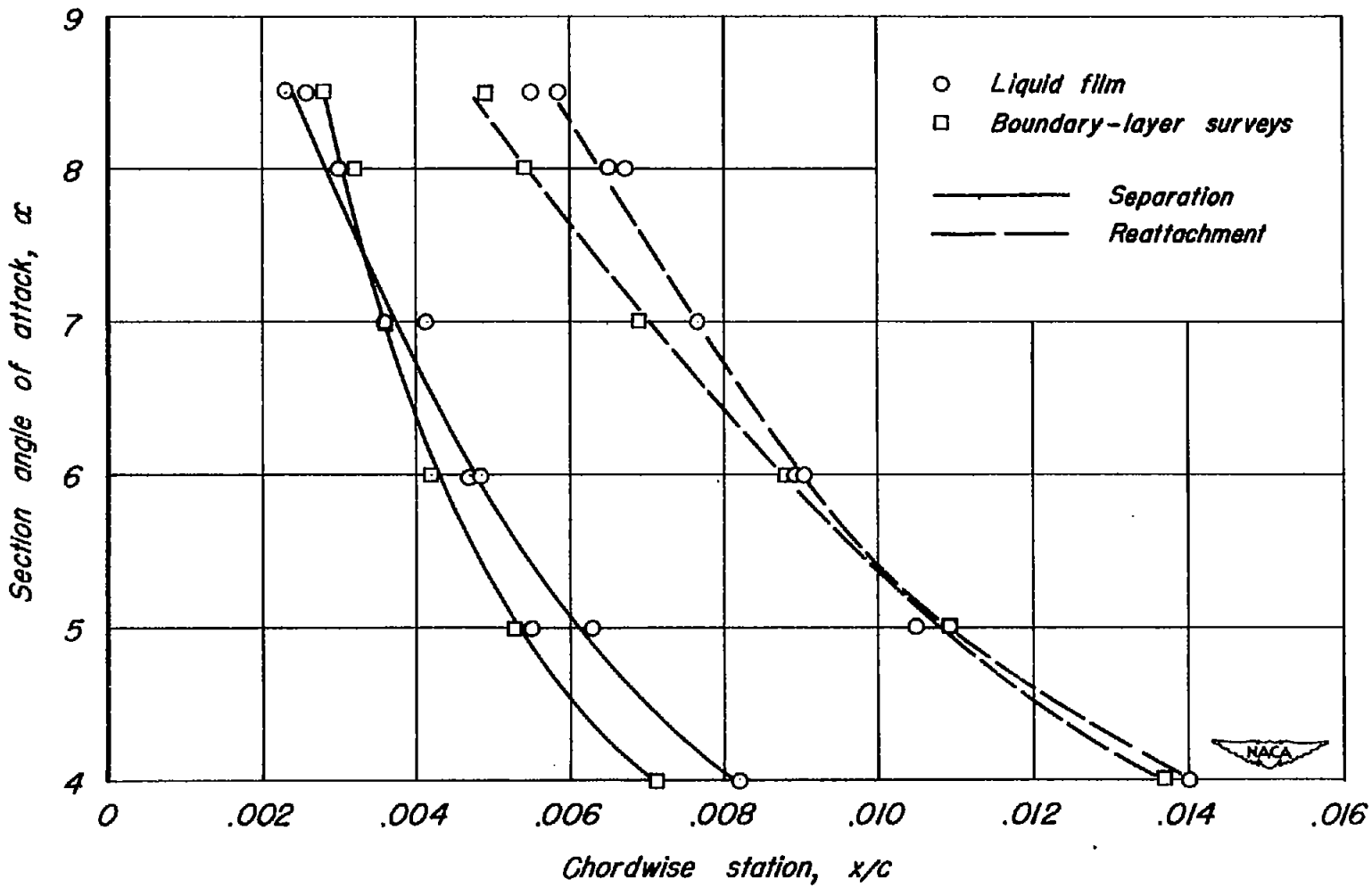

Figure 16.- The extent of the region of separated flow near the leading edge of the NACA 63-009 airfoil section.

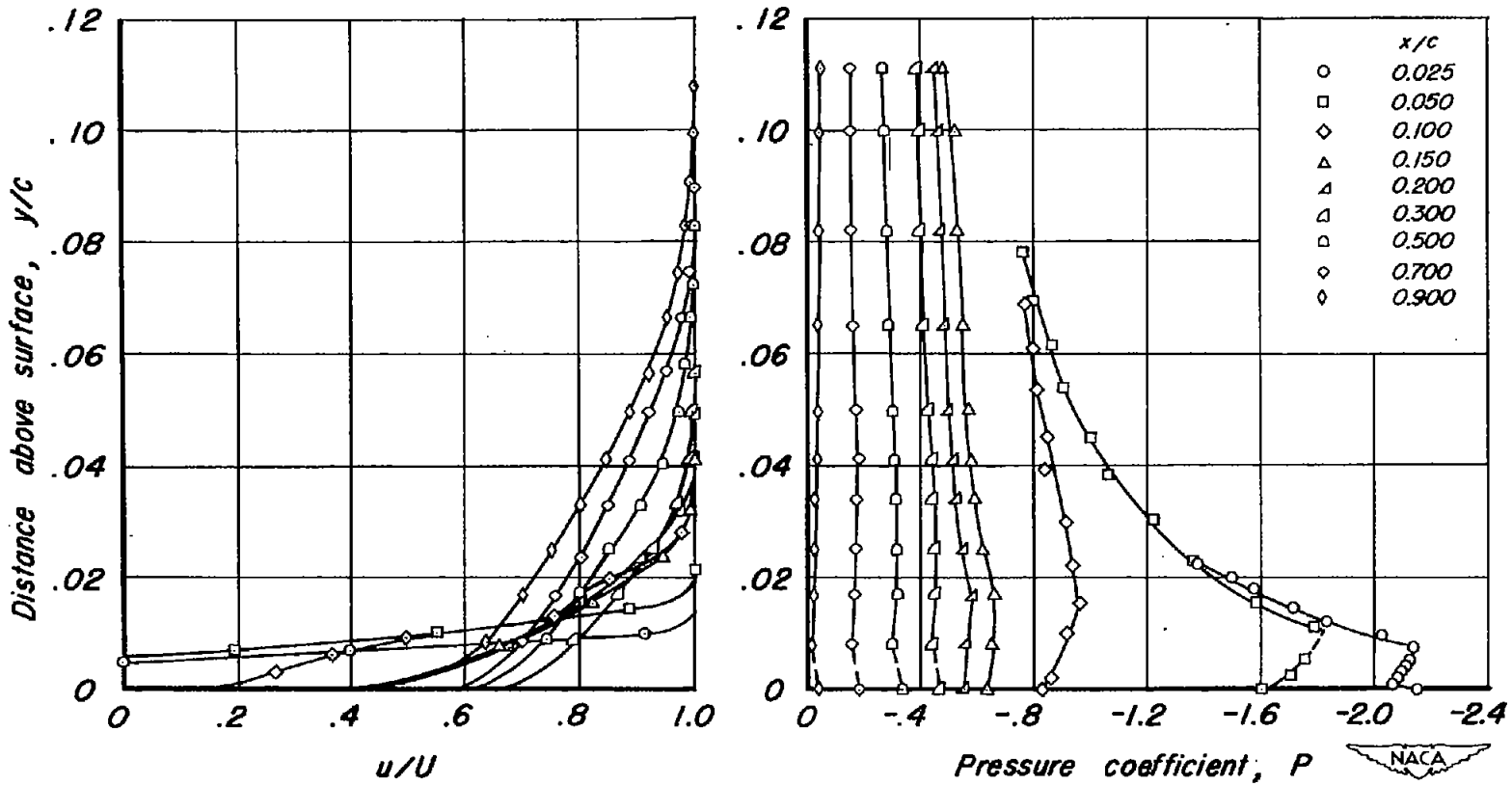

(a) Velocity profile.

(b) Static-pressure profile.

Figure 17.–Boundary-layer velocity and static-pressure profiles. NACA 64A006 airfoil section; $\alpha = 5°$.

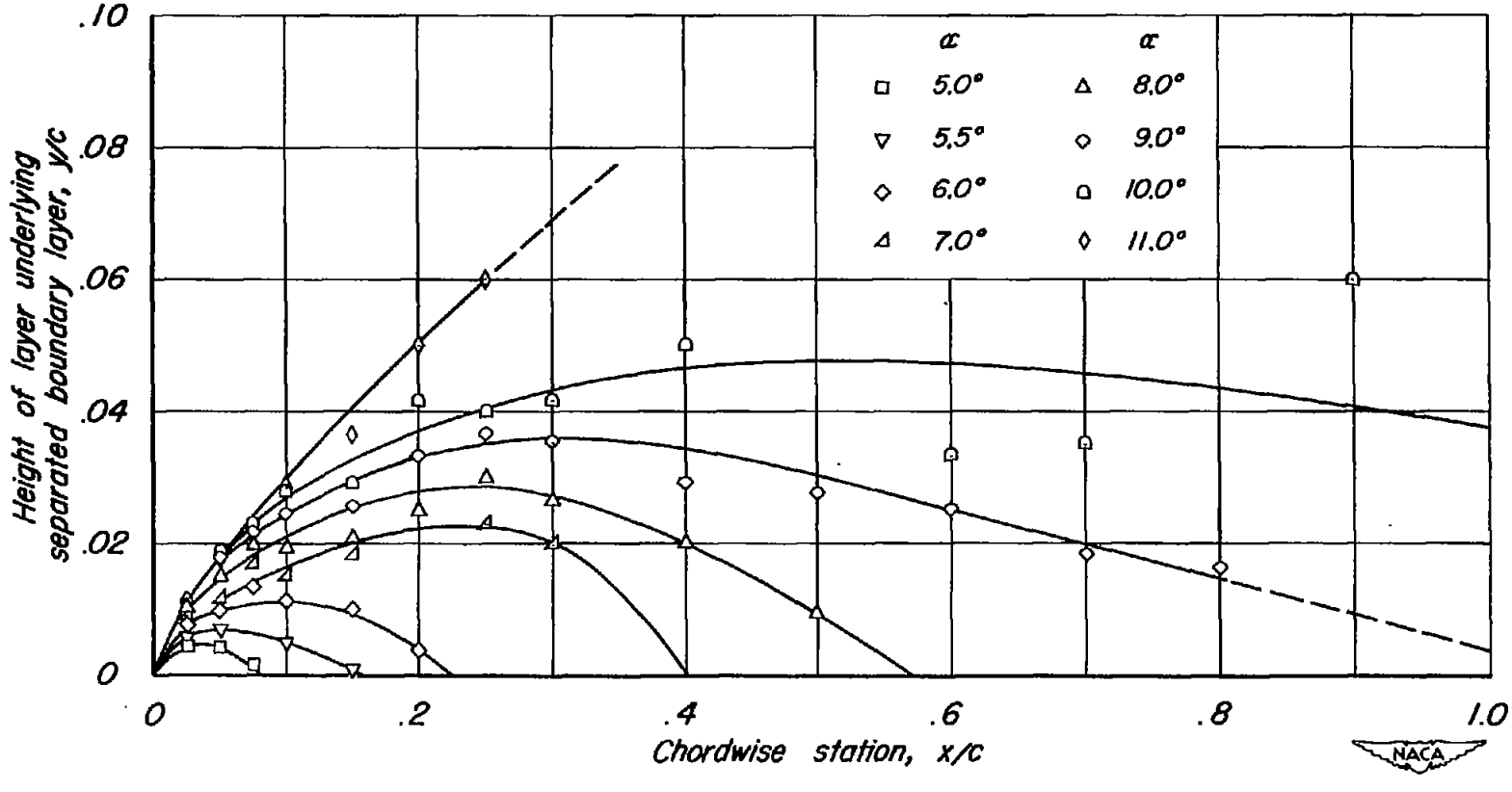

Figure 18.– Growth of the region underlying the separated flow. NACA 64A006 airfoil section.

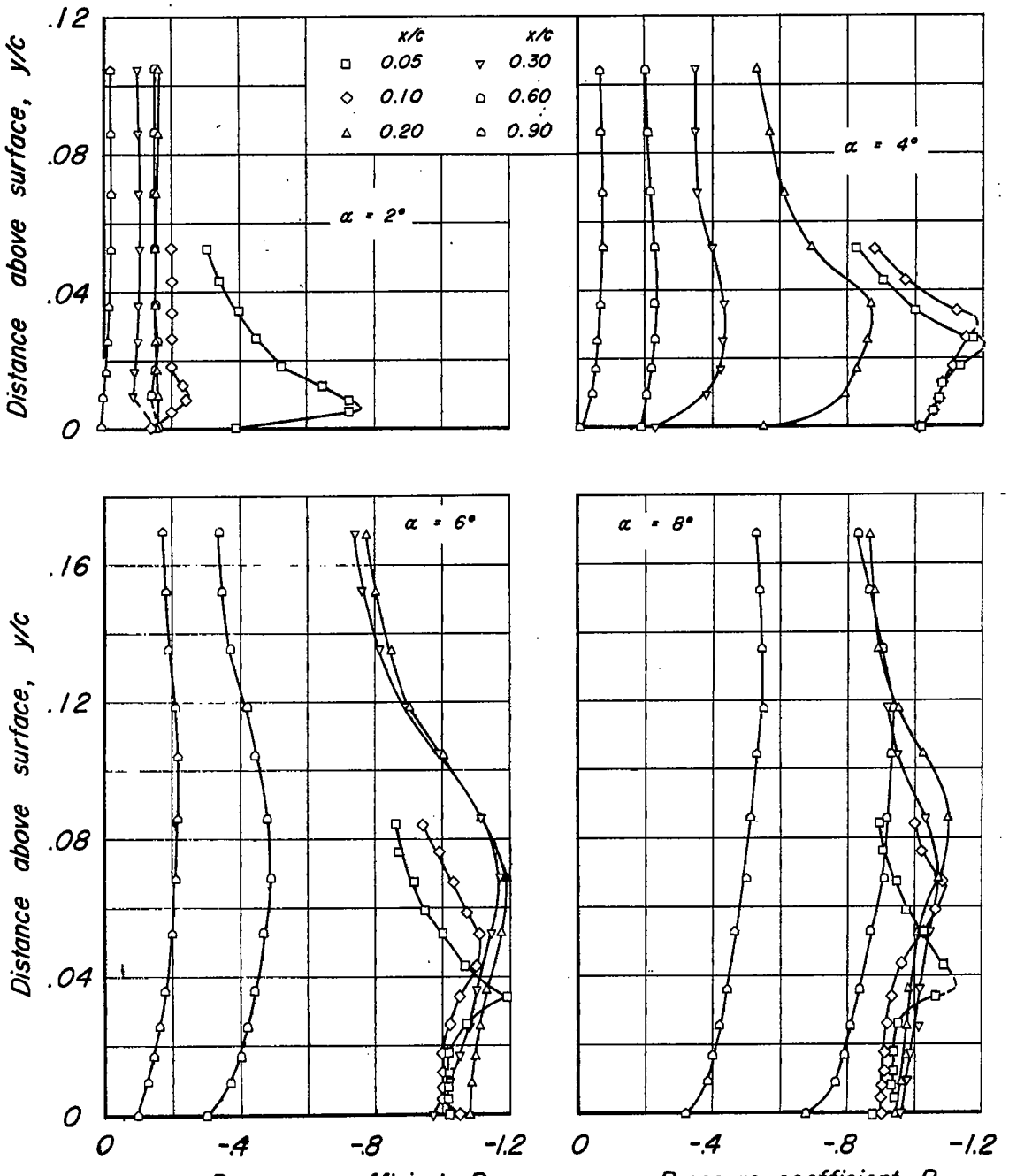

(a) Static-pressure profiles.

Figure 19.- Boundary-layer velocity and static-pressure profiles. 4.23-percent-thick double-wedge airfoil section.

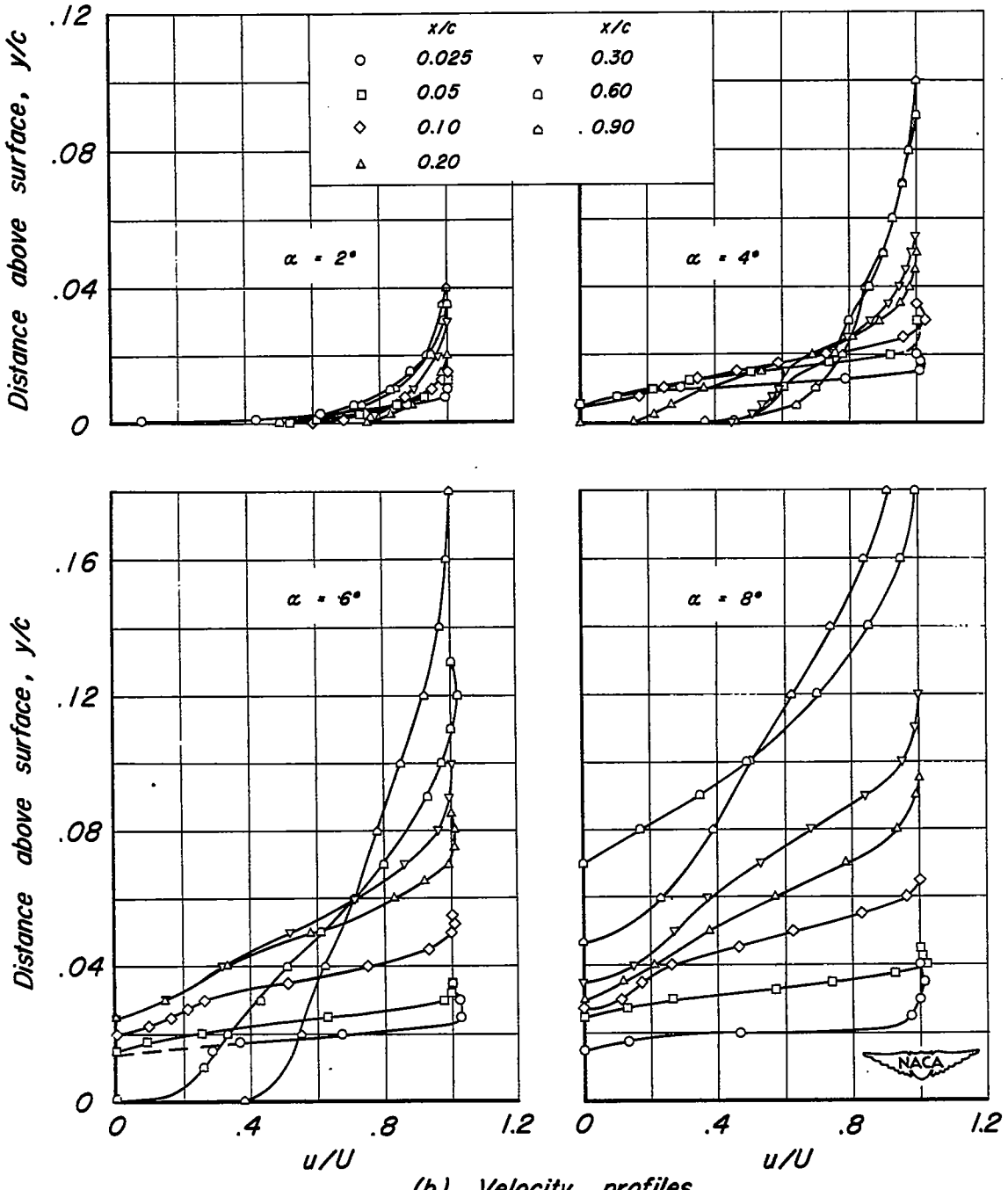

(b) Velocity profiles.

Figure 19.– Concluded.

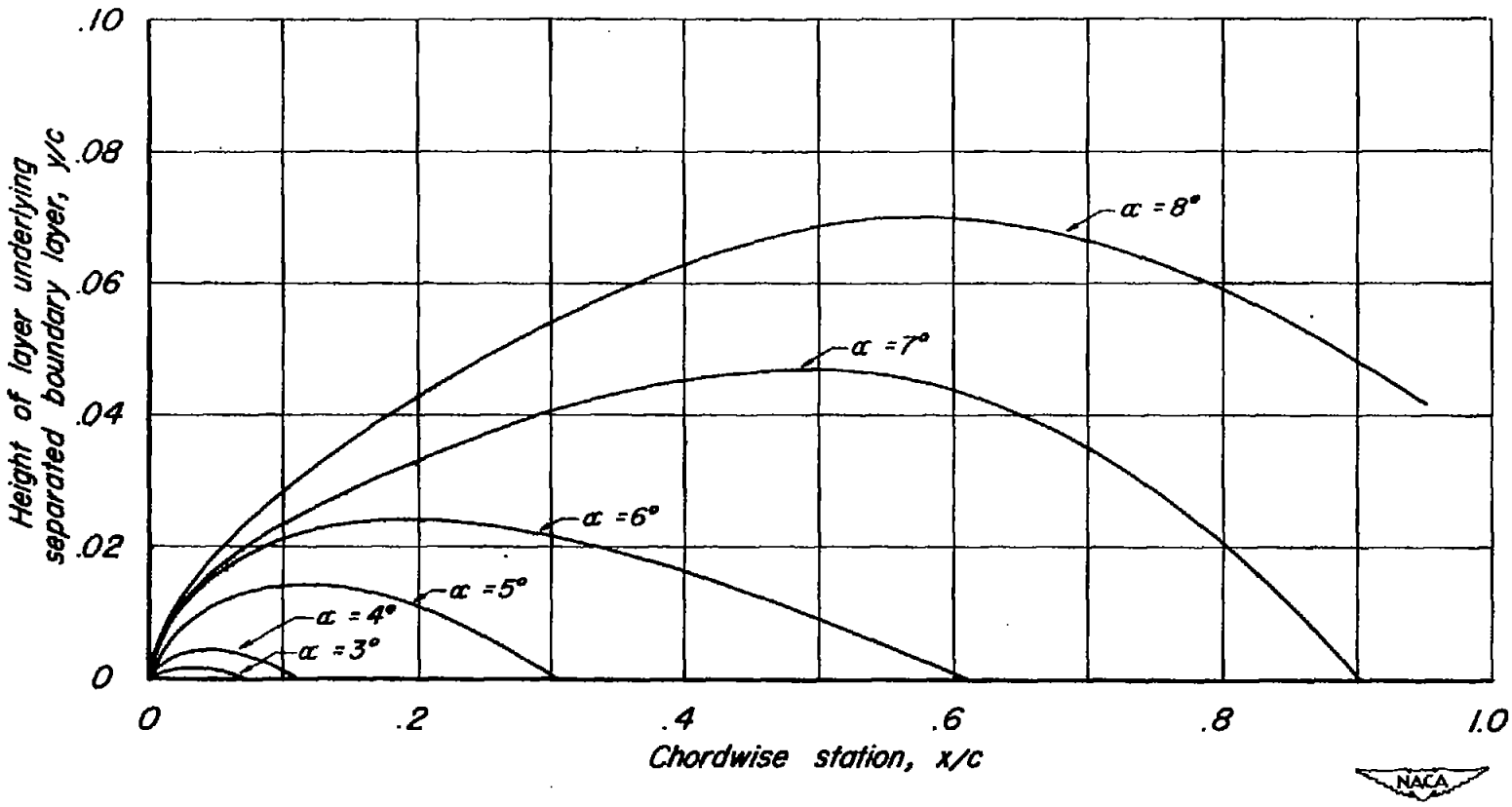

Figure 20.- Growth of the region underlying the separated flow; 4.23-percent-thick double-wedge airfoil section.

NACA-Langley - 9-28-51 - 1000